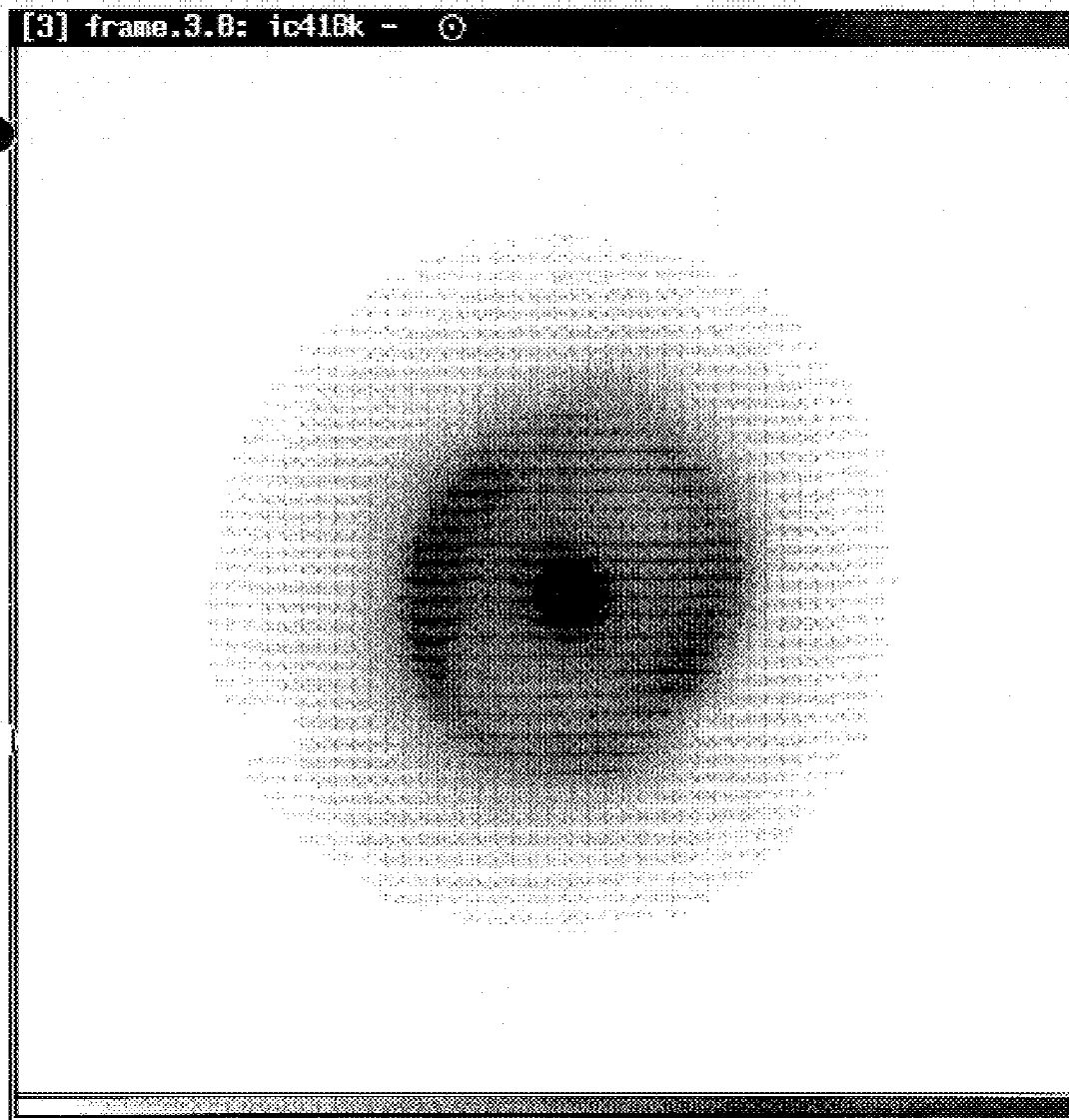Figure 2.21. Grayscale images of IC 418. The gray levels have been selected in each image to show the nebular structure, saturating the central star.
2.21a. IC 418 J grayscale image. The main lobe appears as a dark condensation on the NE portion of the ring. This lobe extends to a point directly N of the central star.

2.21b. IC 418 grayscale image at K. The two lobes are visible in the ring, primarily to the E and W of the central star. The halo is seen to extend beyond the nebula. The "hole" in the left side of the nebula in the outer gray level is due to a faint star in the off-source field.
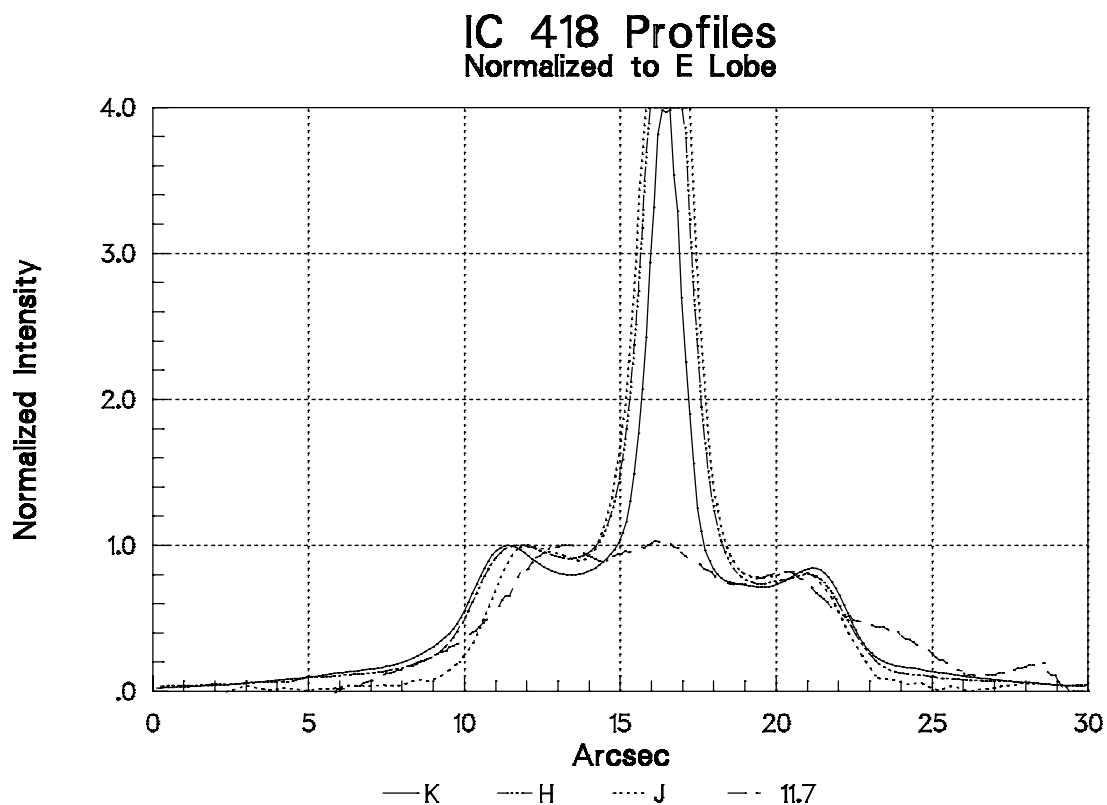
IC 418 Profiles
Normalized to E Lobe

Figure 2.22. Profiles of IC 418 through the major lobes (PA = 70°). The profiles have been normalized so that the NE lobe peak is 1.0, and the profiles aligned to the central star. Each wavelength is assigned a different line type, shown below the figure. The K image profile has the largest spatial extent, followed by the H, J, and 11.7 μm image profiles.
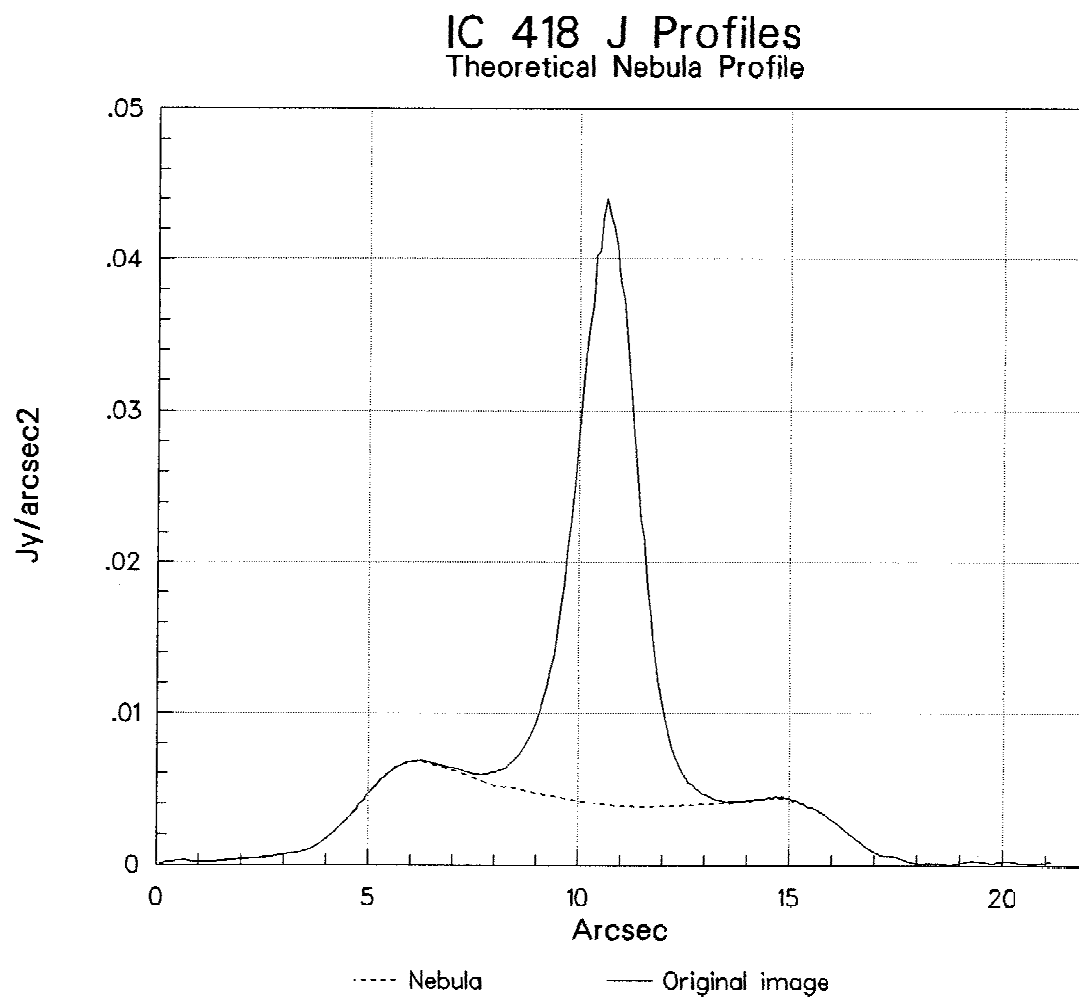
Figure 2.23. Theoretical nebula profile for IC 418, J image. The solid line is the profile from Figure 2.22. The dotted line below the standard star is the assumed profile of the flux from the outer nebular shell alone, without the emission from near the central star.
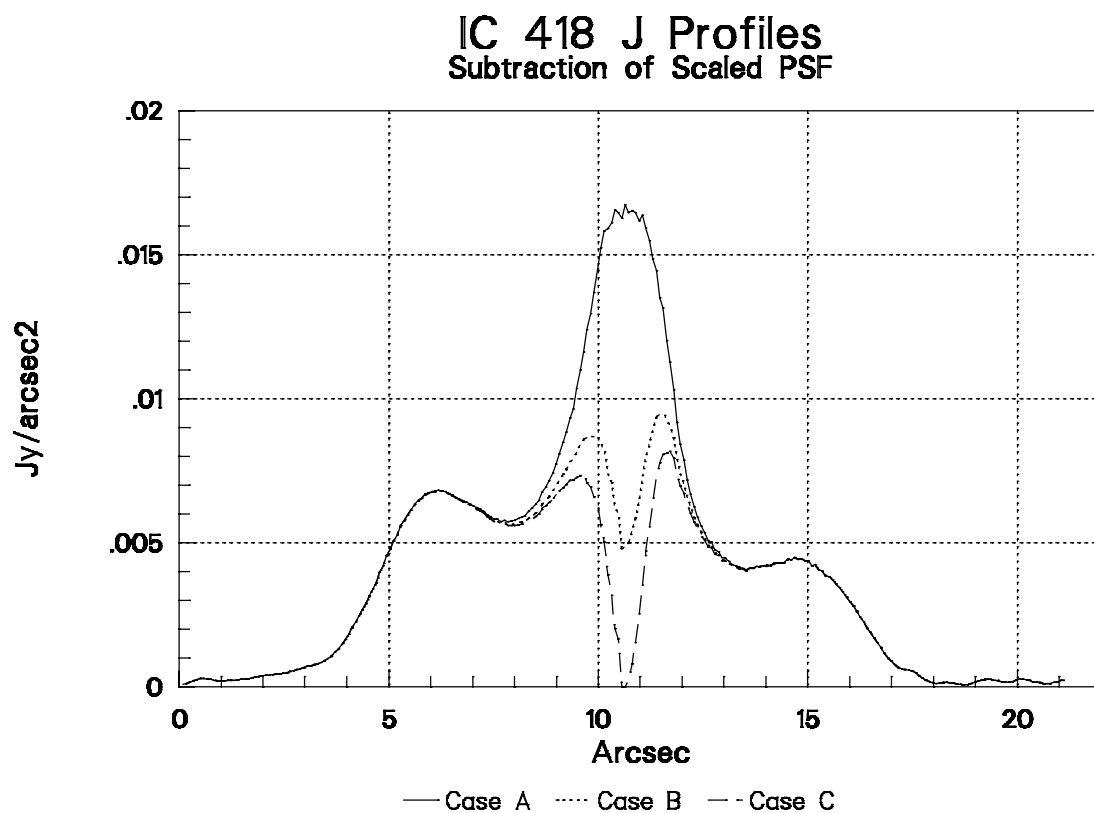
Figure 2.24. PSF-subtracted profiles of IC 418, showing different central star subtractions. In each figure, the solid line is the central star scaled so that there is no central hole. The dotted line is the central star subtracted to the level of the theoretical outer shell profile, as shown above in Figure 2.23. The dashed line is the peak of the star subtracted to the zero level.
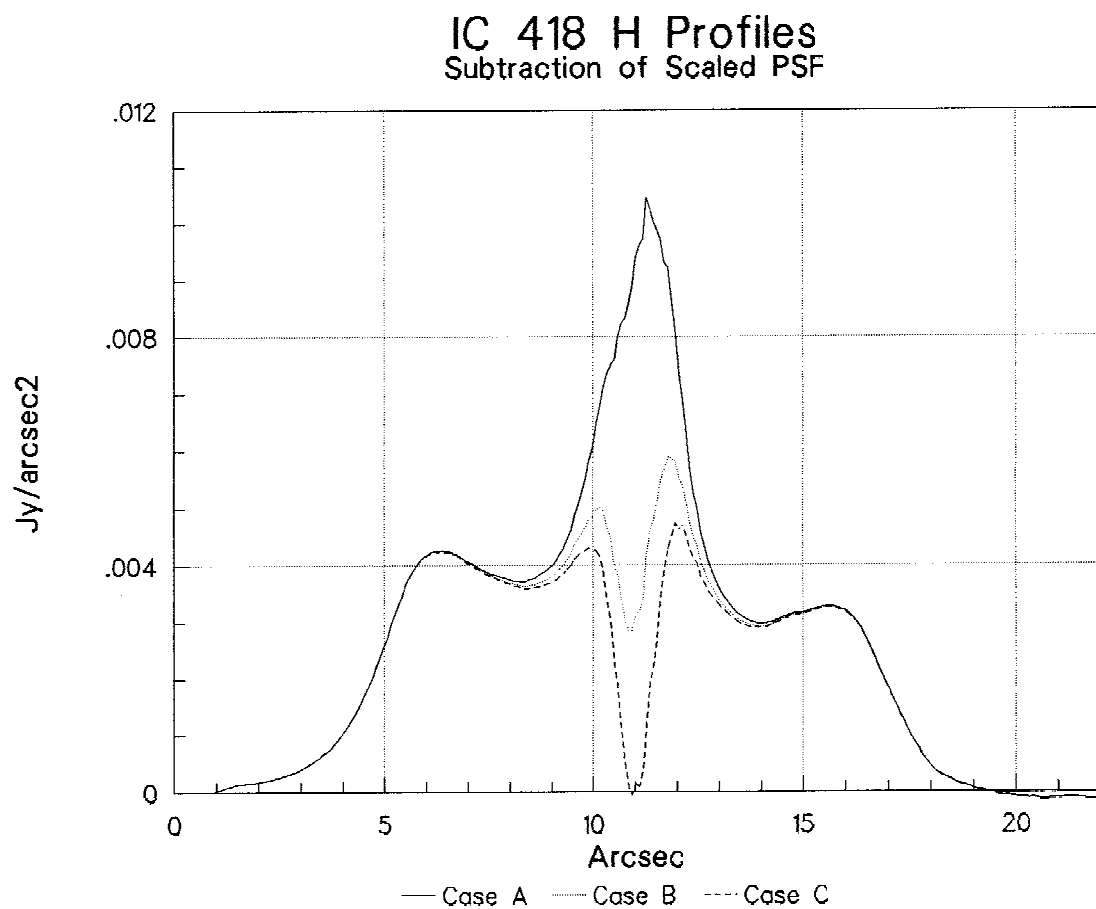2.24a. IC 418 J profiles.

IC 418 H Profiles
Subtraction of Scaled PSF

Figure 2.24b. IC 418 H profiles (see main caption to Figure 2.24).

IC 418 K Profiles
Subtraction of PSF

Figure 2.24c. IC 418 K profiles (see main caption to Figure 2.24).
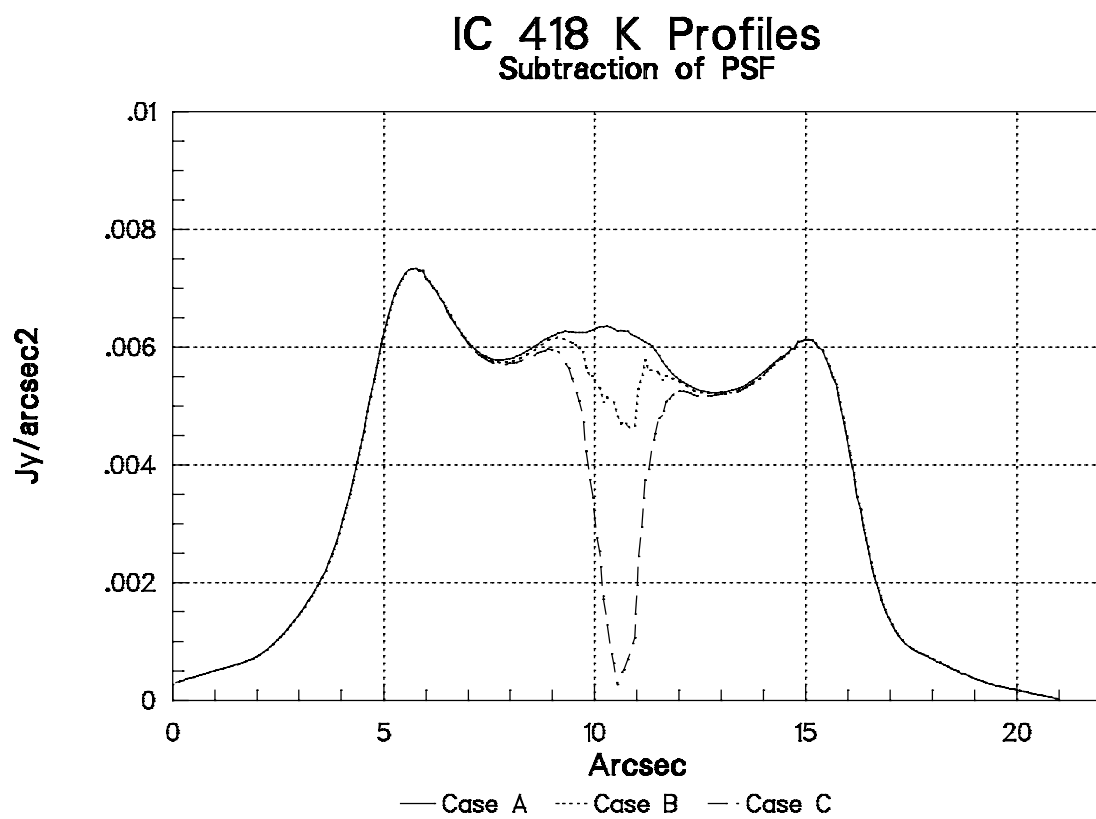
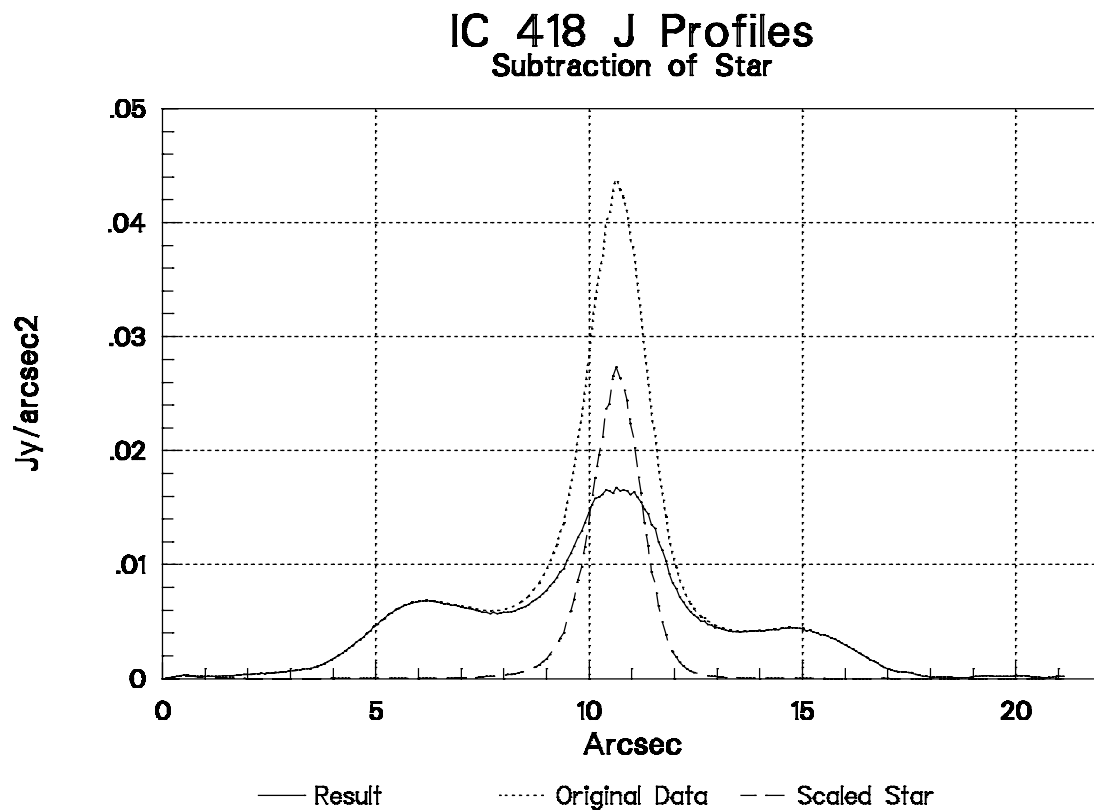## IC 418 J Profiles
Subtraction of Star

Figure 2.25. PSF-subtracted profiles of IC 418. These profiles show the original data (dotted line), the scaled standard star (dashed line), and the resulting profile when the star is subtracted (solid line). The solid line in this figure is the same as the solid line in Figure 2.24.
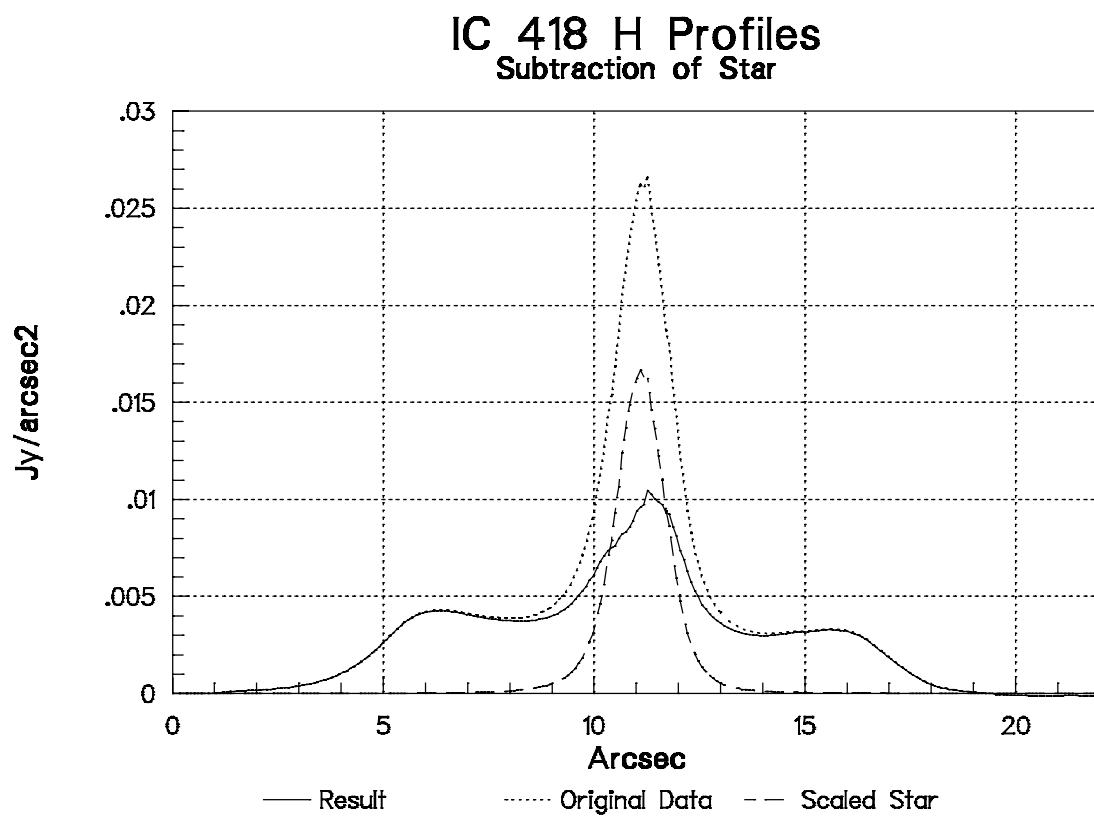
2.25a. IC 418 J PSF-subtracted profiles.

IC 418 H Profiles
Subtraction of Star

Figure 2.25b. IC 418 H PSF-subtracted profiles (see main caption of Figure 2.25).

IC 418 K Profiles
Subtraction of Star

Figure 2.25c. IC 418 K PSF-subtracted profiles (see main caption to Figure 2.25).

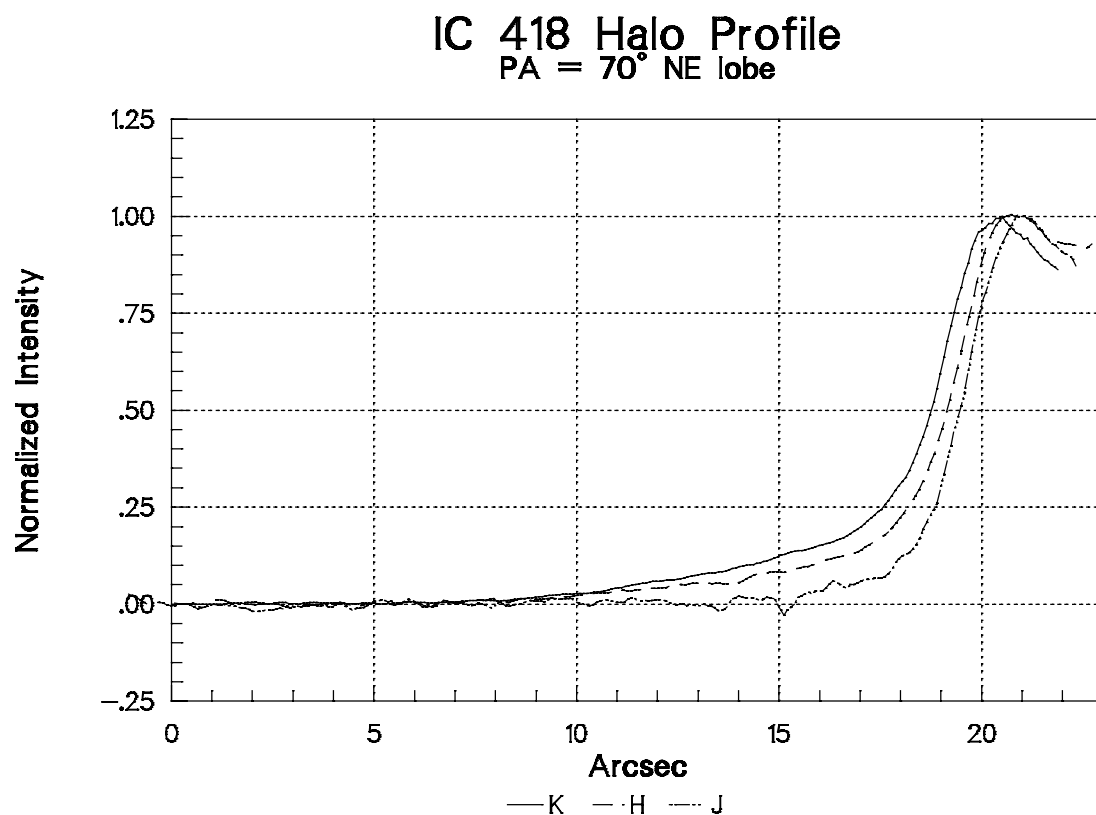## IC 418 Halo Profile
PA = 70° NE lobe

Figure 2.26. Profiles of IC 418 halo, in the same direction as previous profiles, extending further to the NE and including the NE lobe peak. The profiles have been aligned on the central star. The profiles show the halo emission in H and K, and the much weaker emission in the J profile beyond the nebular shell.
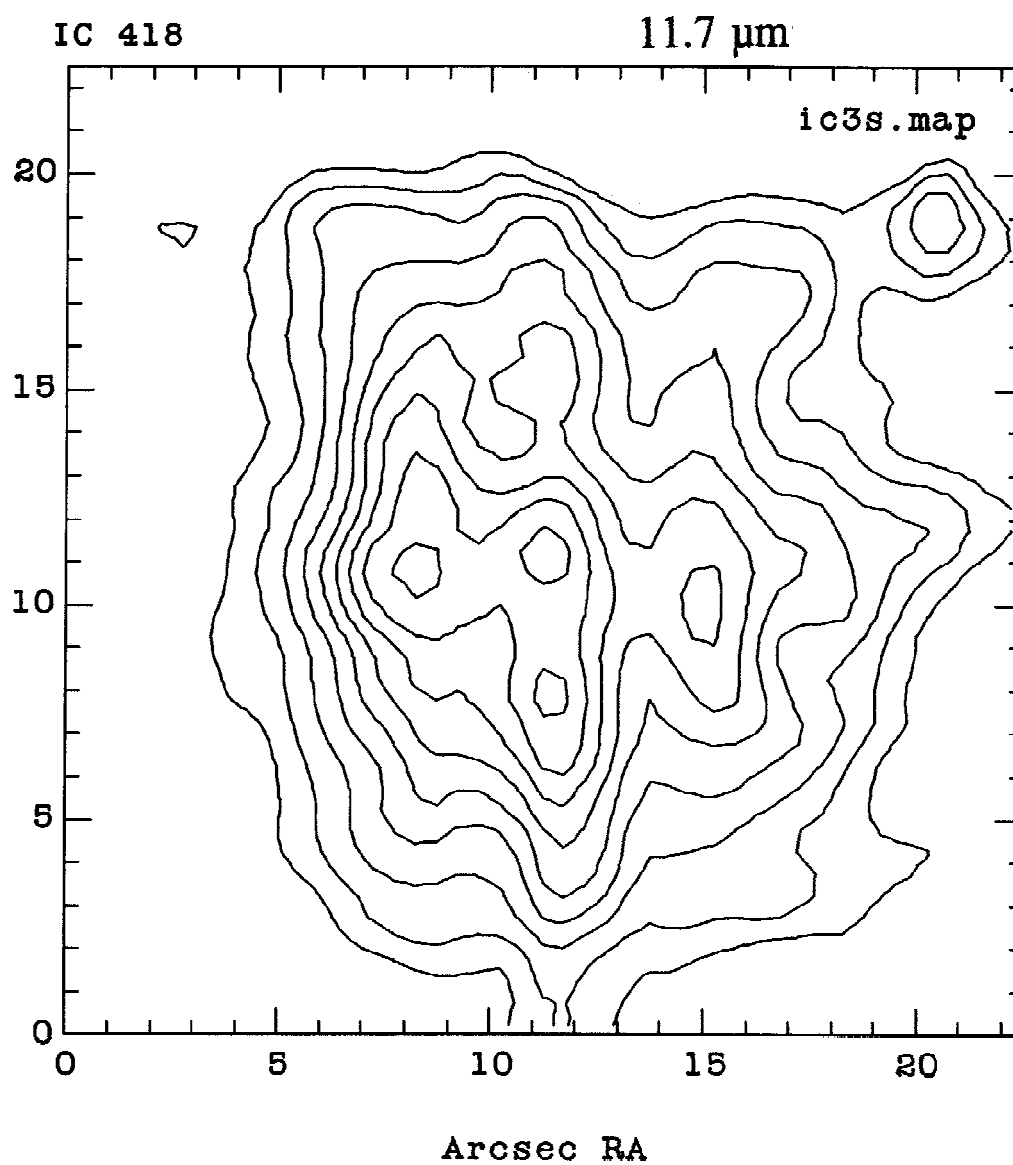
IC 418   11.7 μm

ic3s.map

Arcsec RA

Figure 2.27. Contour image of IC 418 at 11.7 μm, from MIRAC observations. The contour levels are evenly spaced at 140 mJy/arcsec^2 per level, starting at 100 mJy/arcsec^2.
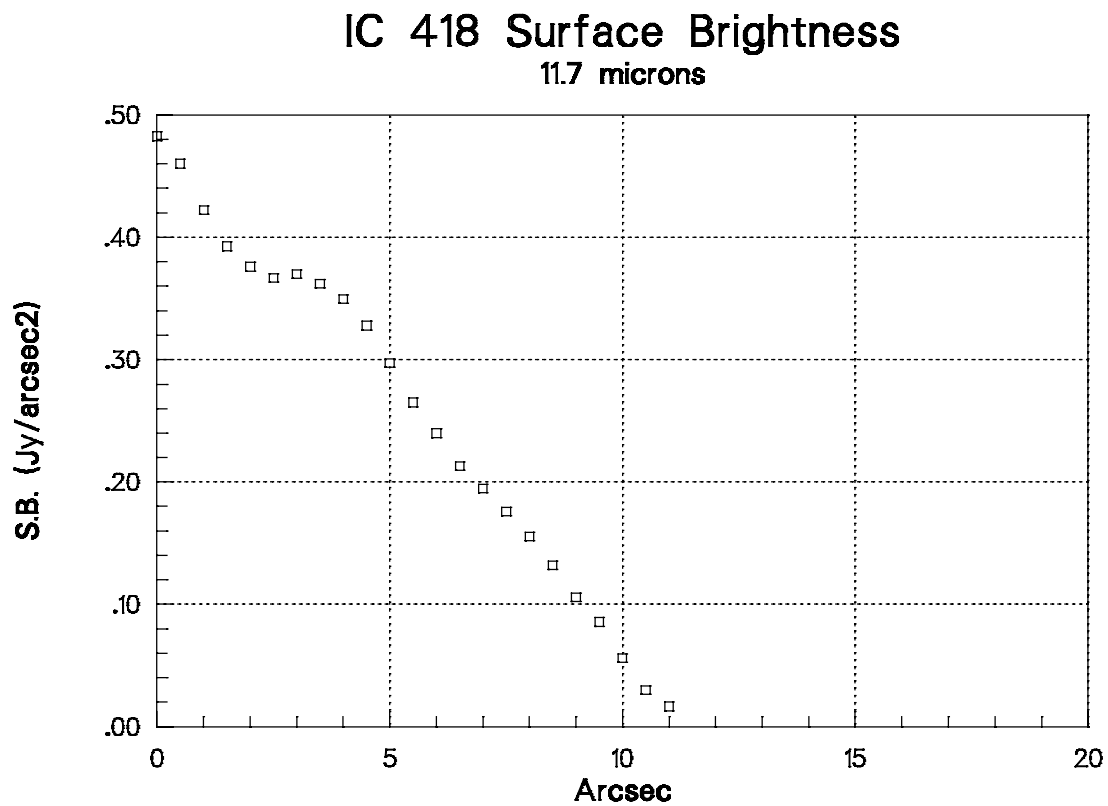
Figure 2.28. Observed surface brightness of IC 418 at 11.7 μm, determined from the image in Figure 2.27. The surface brightness in Jy/arcsec^2 is plotted as a function of distance from the center of the nebula in arcsec.
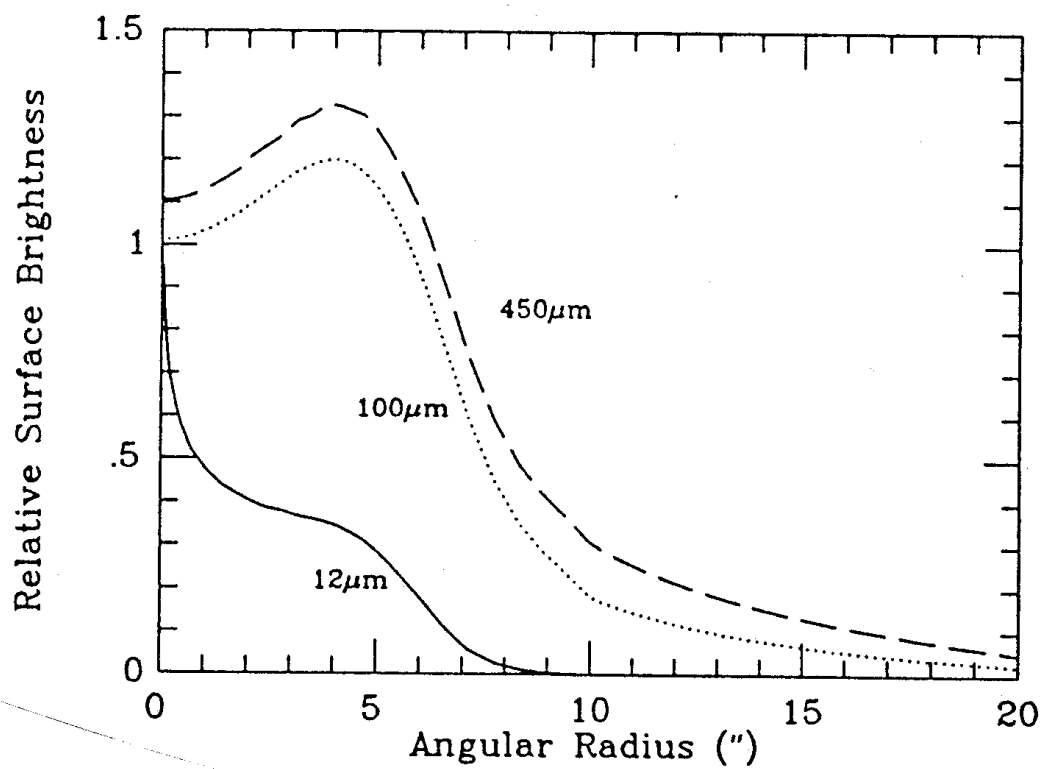
Figure 2.29. Surface brightness of IC 418, from Hoare (1990). This plot is from the amorphous carbon model of IC 418 that includes a neutral halo.
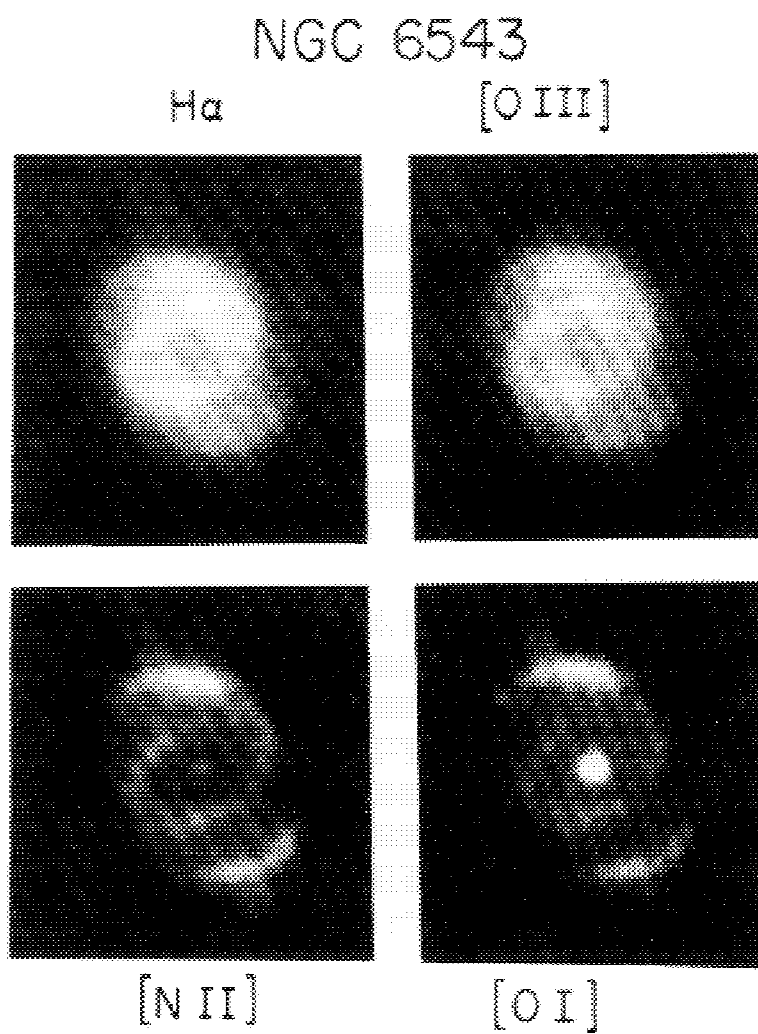
Figure 2.30. Images of the planetary nebula NGC 6543, from Balick and Preston (1987).
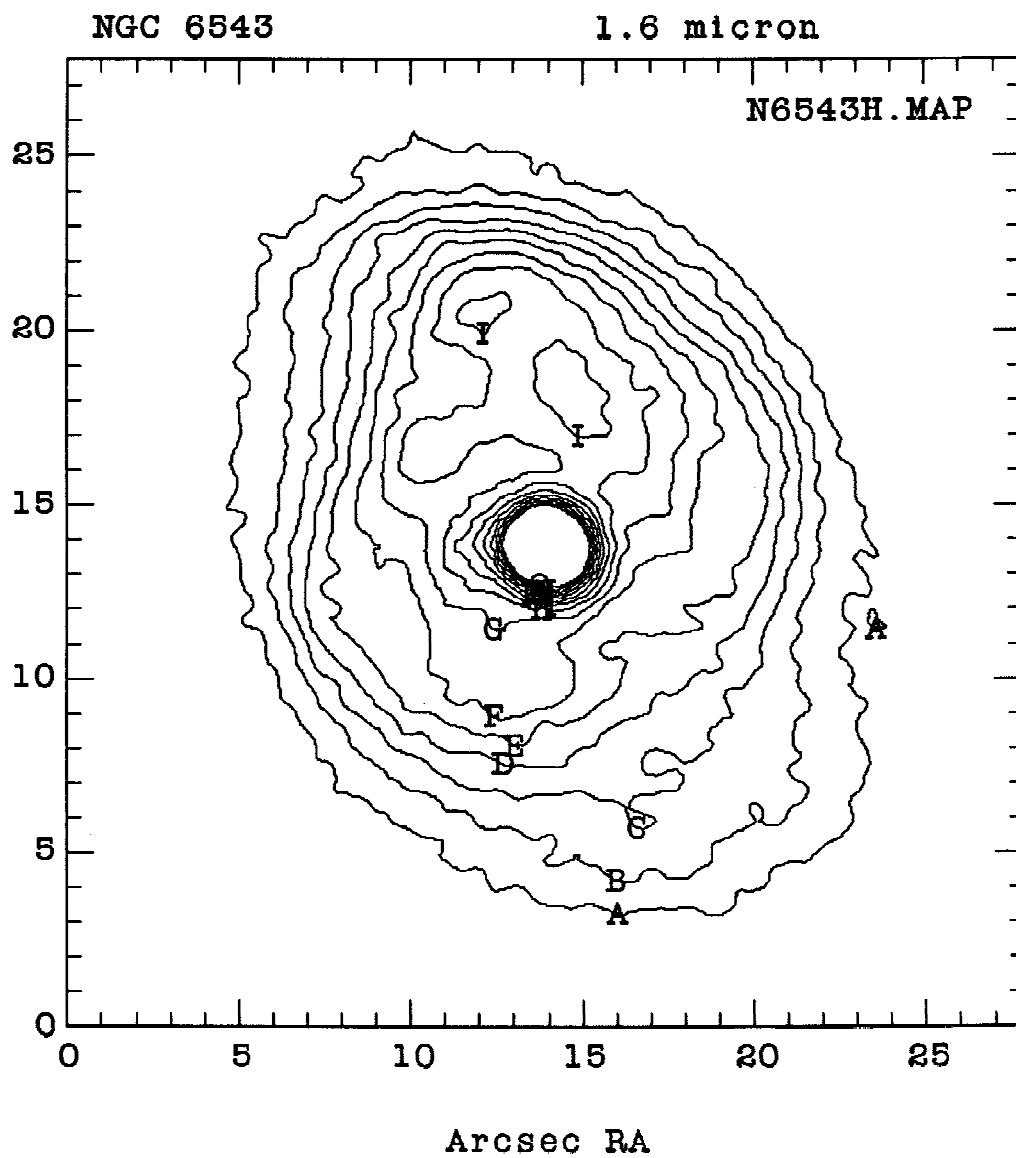
Figure 2.31. Contour images of the planetary nebula NGC 6543. The contour level spacing is at even intervals of .15 mJy/arcsec^2, with a minimum level of .15 mJy/arcsec^2.
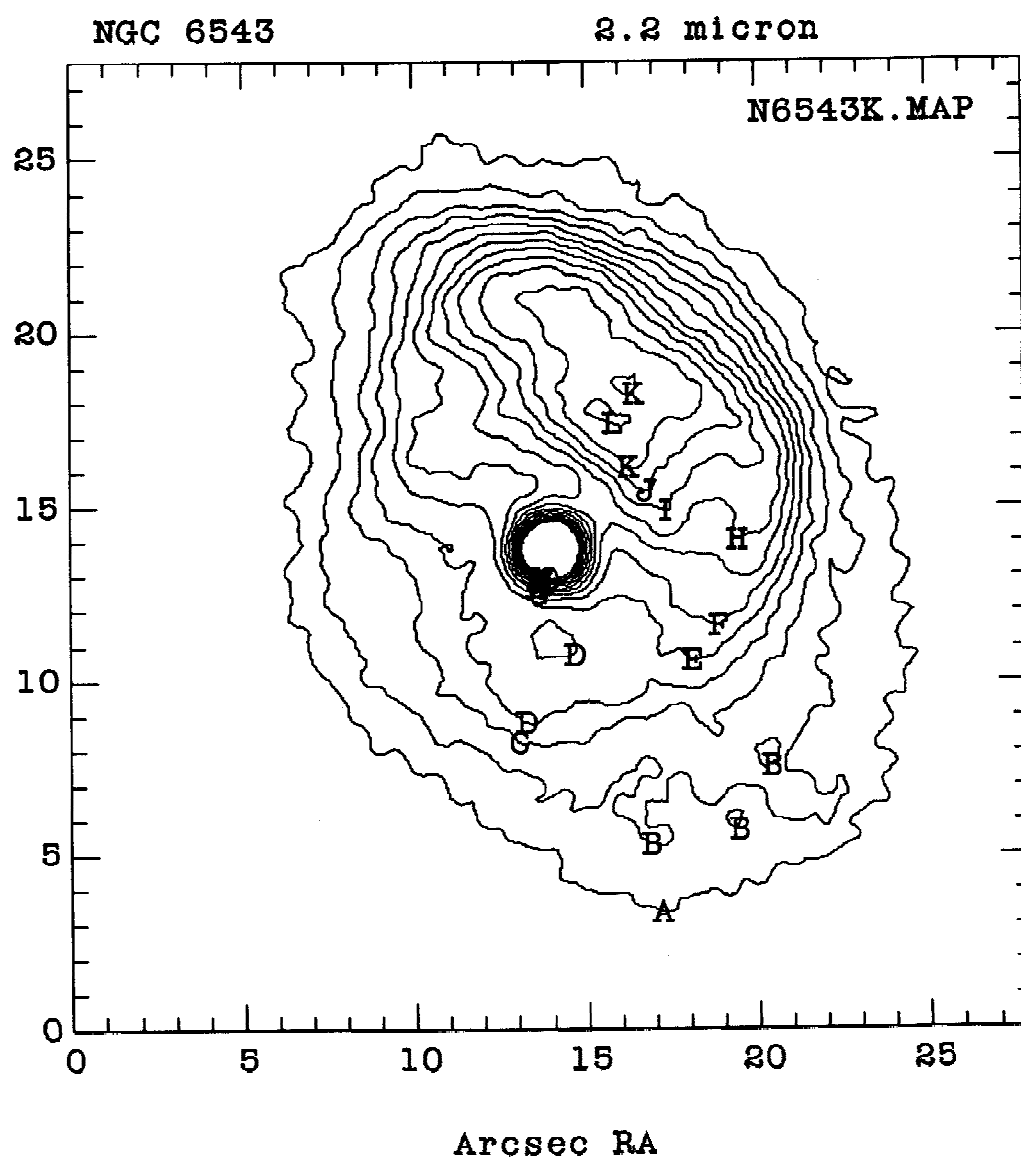
2.31a. NGC 6543 H contour image.

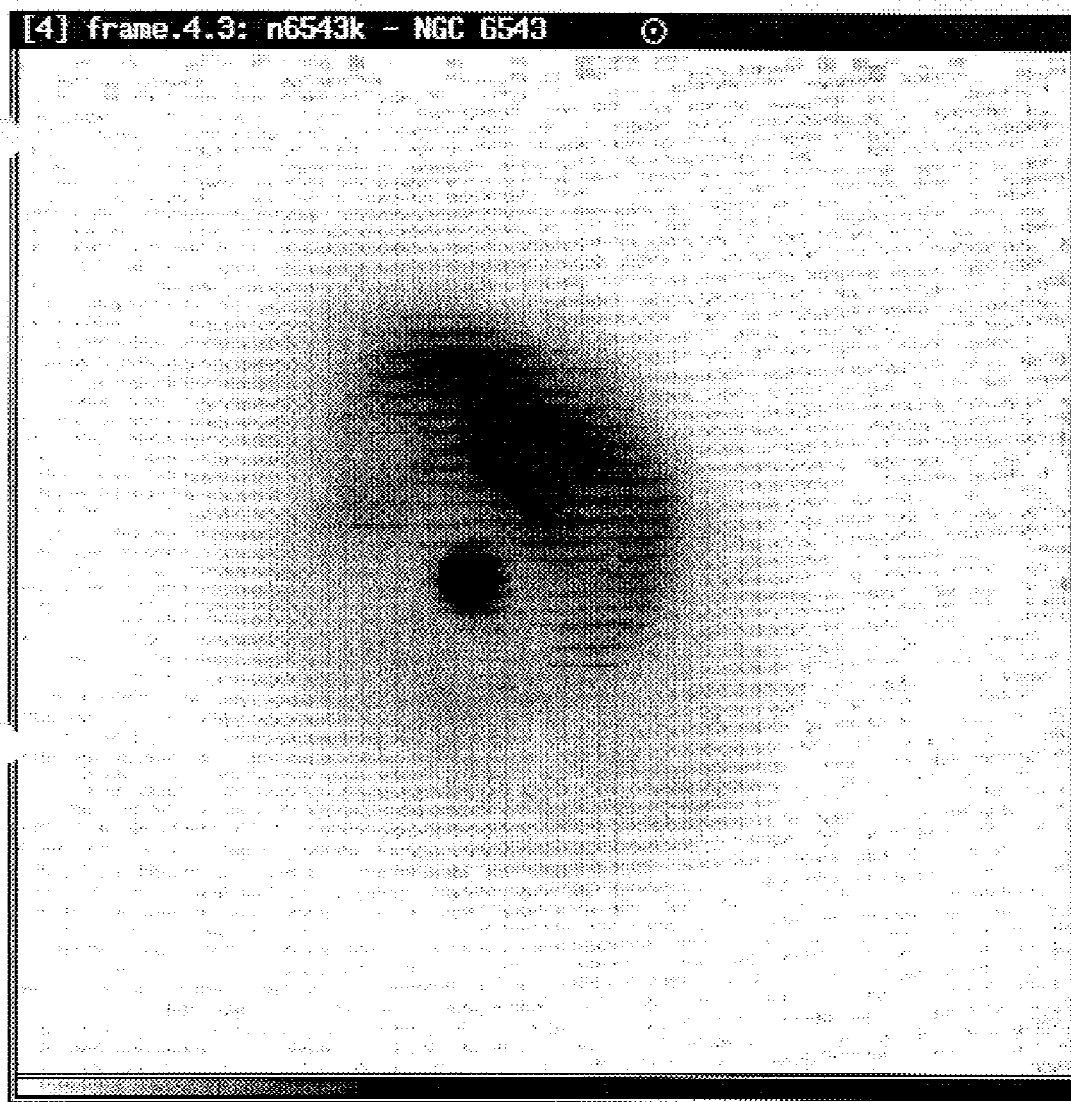Figure 2.31b. NGC 6543 K contour image (see main caption of Figure 2.31).

Figure 2.32. Grayscale image of NGC 6543 in the K filter. The gray levels have been set to saturate the bright lobe, so that the faint structure is visible. The faint halo enveloping the bright inner shells is also visible.
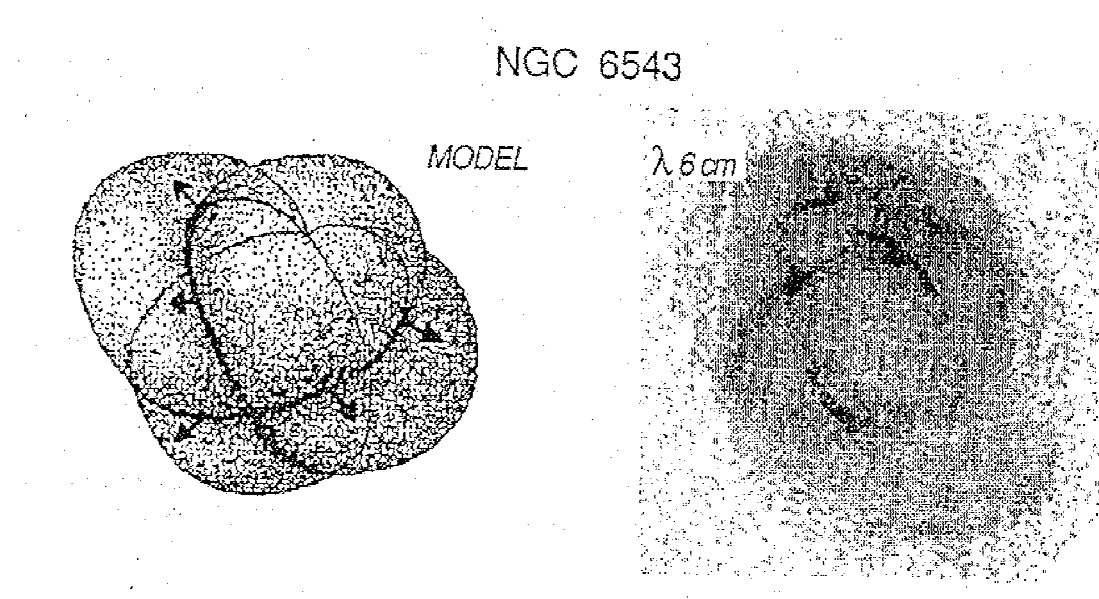
Figure 2.33. Model of the structure of NGC 6543, from Balick and Preston (1987). The model consists of four separate lobes, at the inclination angle shown. The observed morphology results from an intensity enhancement along the points where the lobes intersect. The 6 cm image of NGC 6543 is shown for comparison.
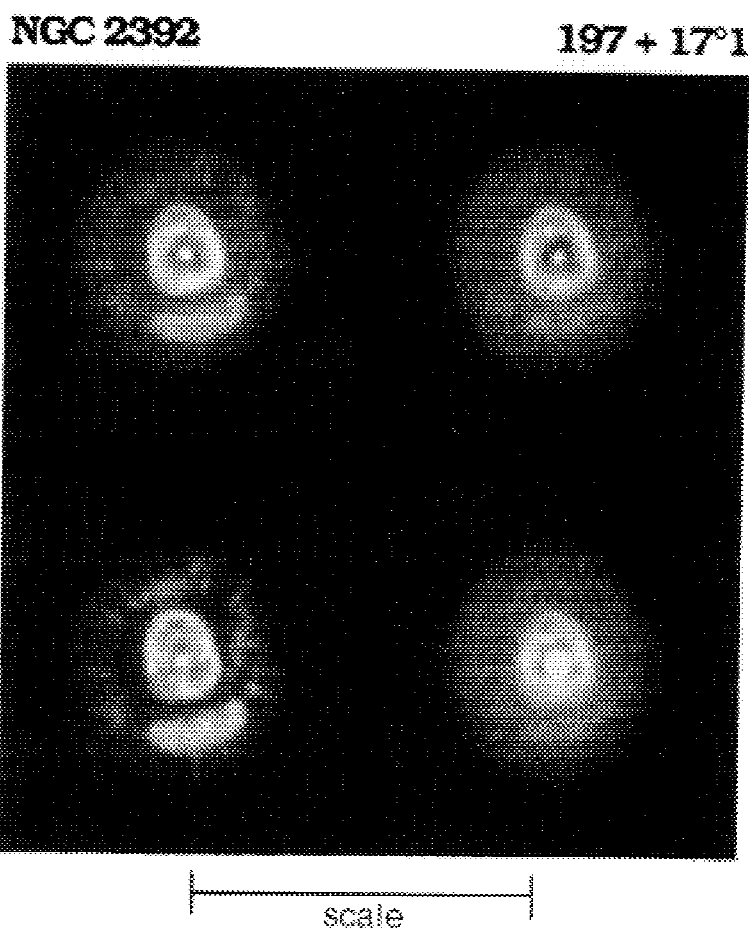
Figure 2.34. CCD images of NGC 2392, from Balick (1987). The scale bar shown has a length of 75". The images were taken at the wavelengths of the following lines, in the order clockwise from the upper left: Hα, [OIII], He II, and [NII].

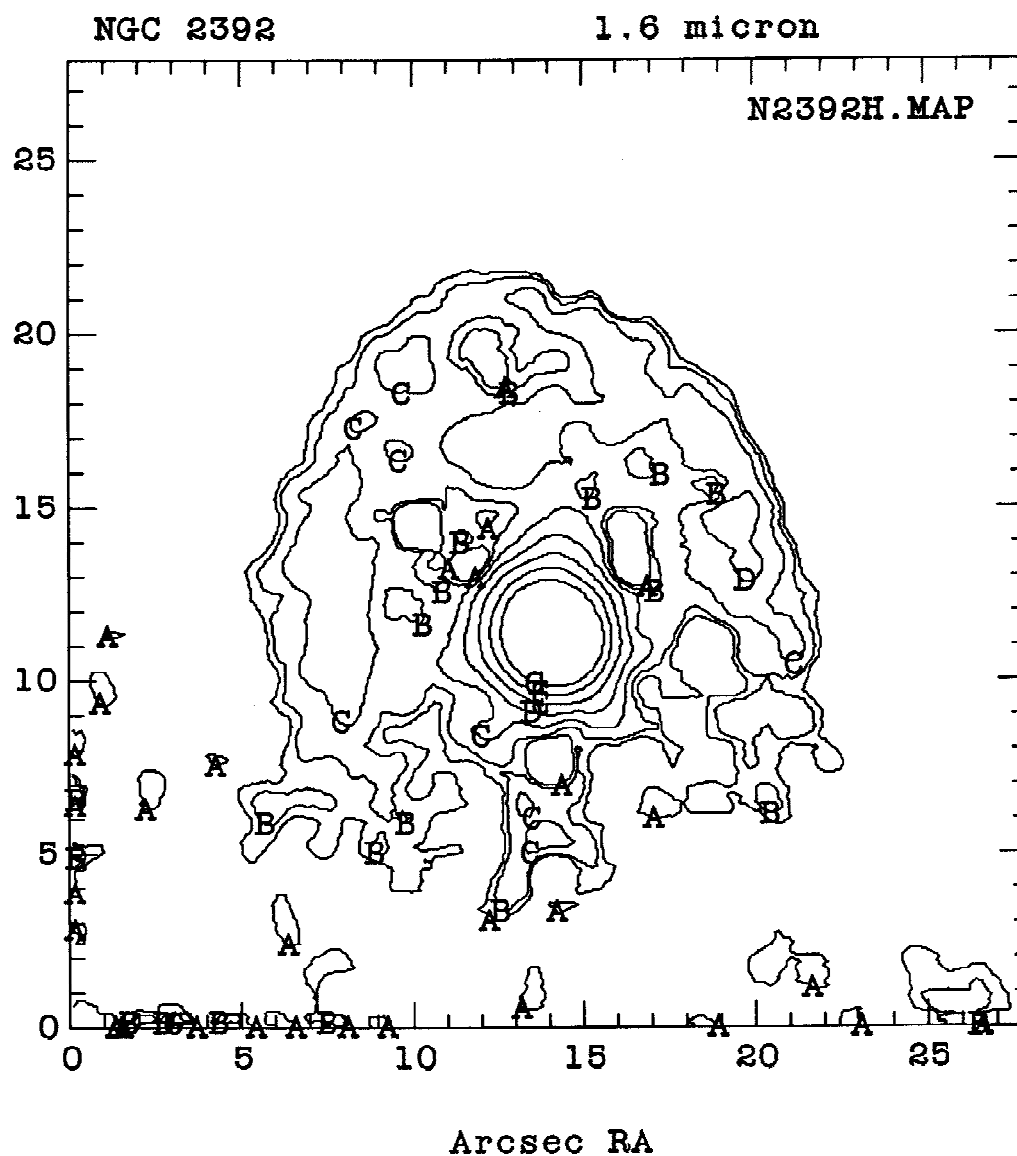

Figure 2.35. Contour images of NGC 2392. The contour levels are logarithmically spaced, with the levels as given for each image. The contour levels do not show the peak of the central star.

2.35a. NGC 2392 H contour image. The contour levels are (in mJy): A = .07, B = .102, C = .150, D = .218, E = .320, F = .468, G = .684.
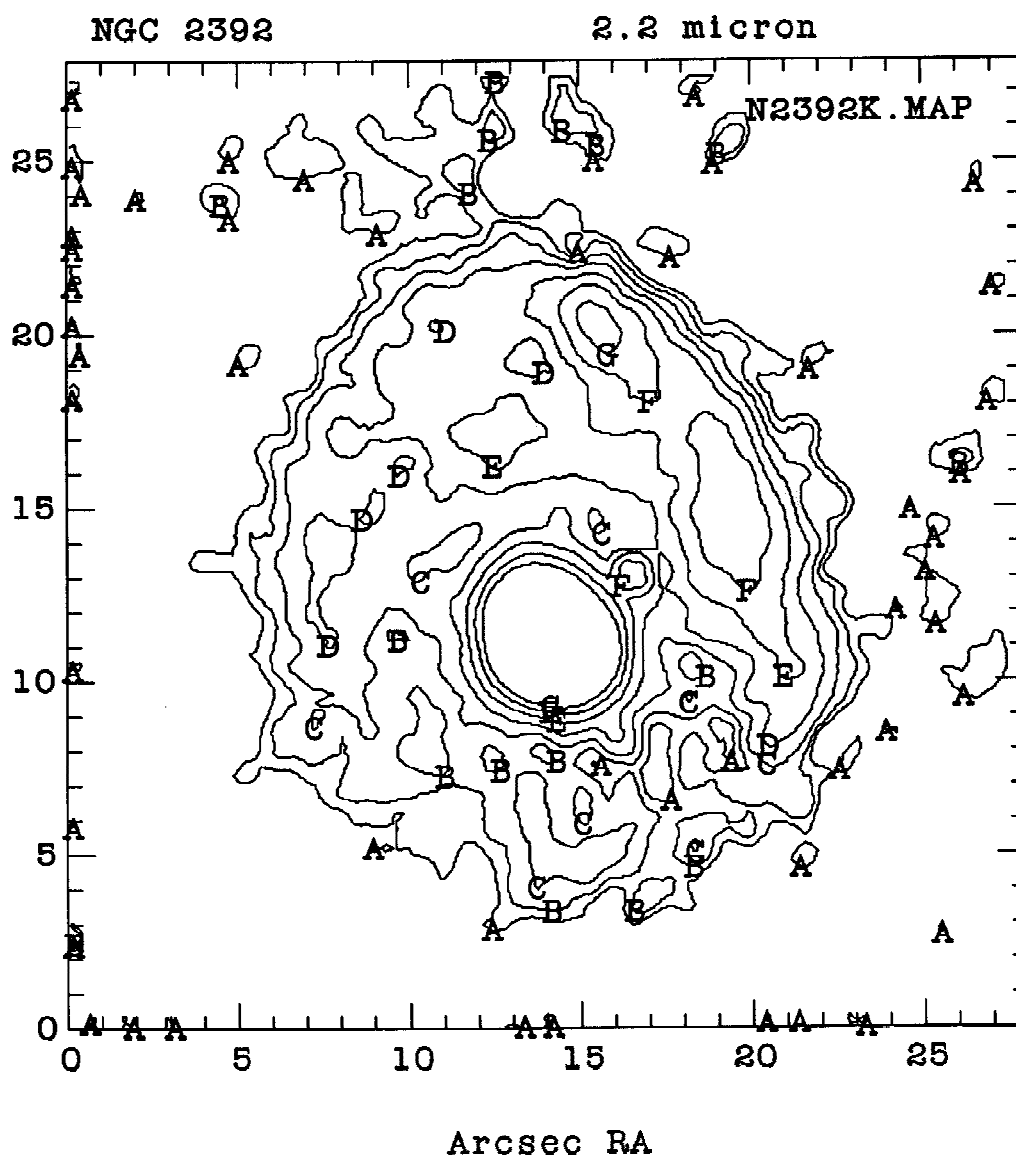
Figure 2.35b. NGC 2392 K contour image. The contour levels are (in mJy): A = .07, B = .102, C = .150, D = .218, E = .320, F = .468, G = .684.

Figure 2.36. Grayscale images of NGC 2392. The bar shown at the bottom of the figure has a length of 10". The gray levels have been chosen to show the nebular structure, so the central star is saturated in this image.
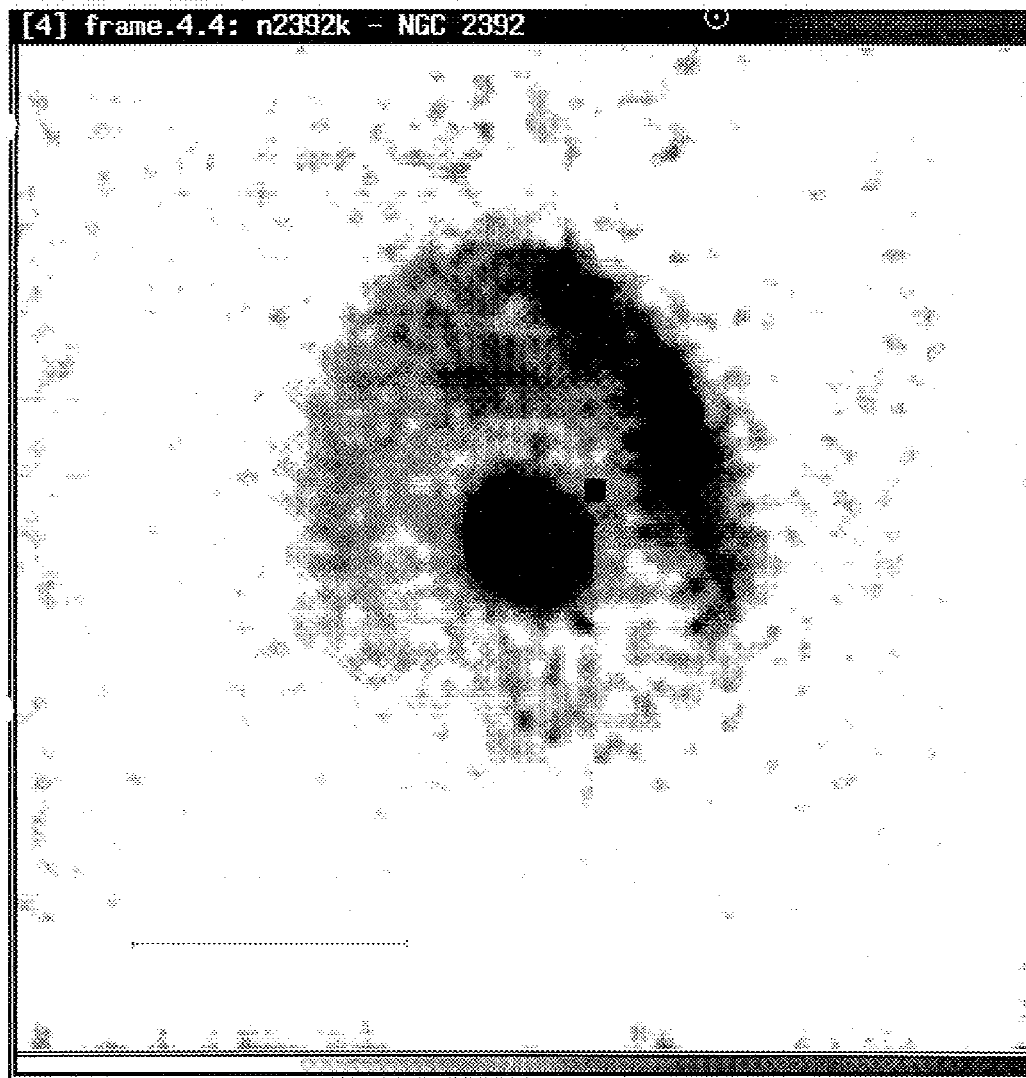2.36a. NGC 2392 H grayscale image.

Figure 2.36b. NGC 2392 K grayscale image (see main caption to Figure 2.36).

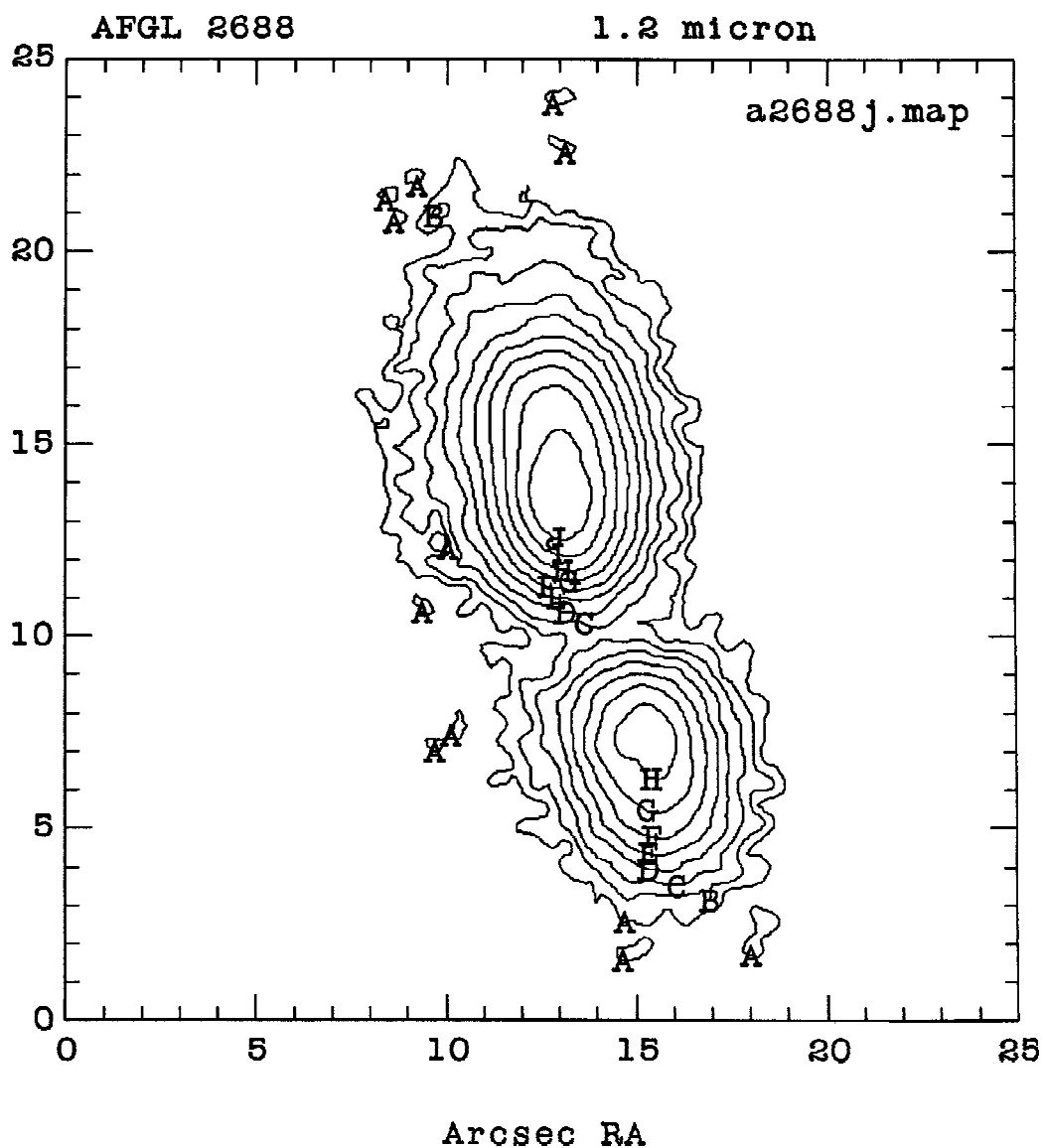Figure 2.37. Optical image of AFGL 2688, from Ney *et. al* (1975).

Figure 2.38. Contour images of AFGL 2688. Contour levels are logarithmically spaced, at the levels given for each image.

2.38a. AFGL 2688 J contour image. Contour levels are set to the following values, in mJy/arcsec^2: A = .3, B = .447, C = .668, D = .998, E = 1.49, F = 2.22, G = 3.32, H = 4.95, I = 7.40, J = 11.0.
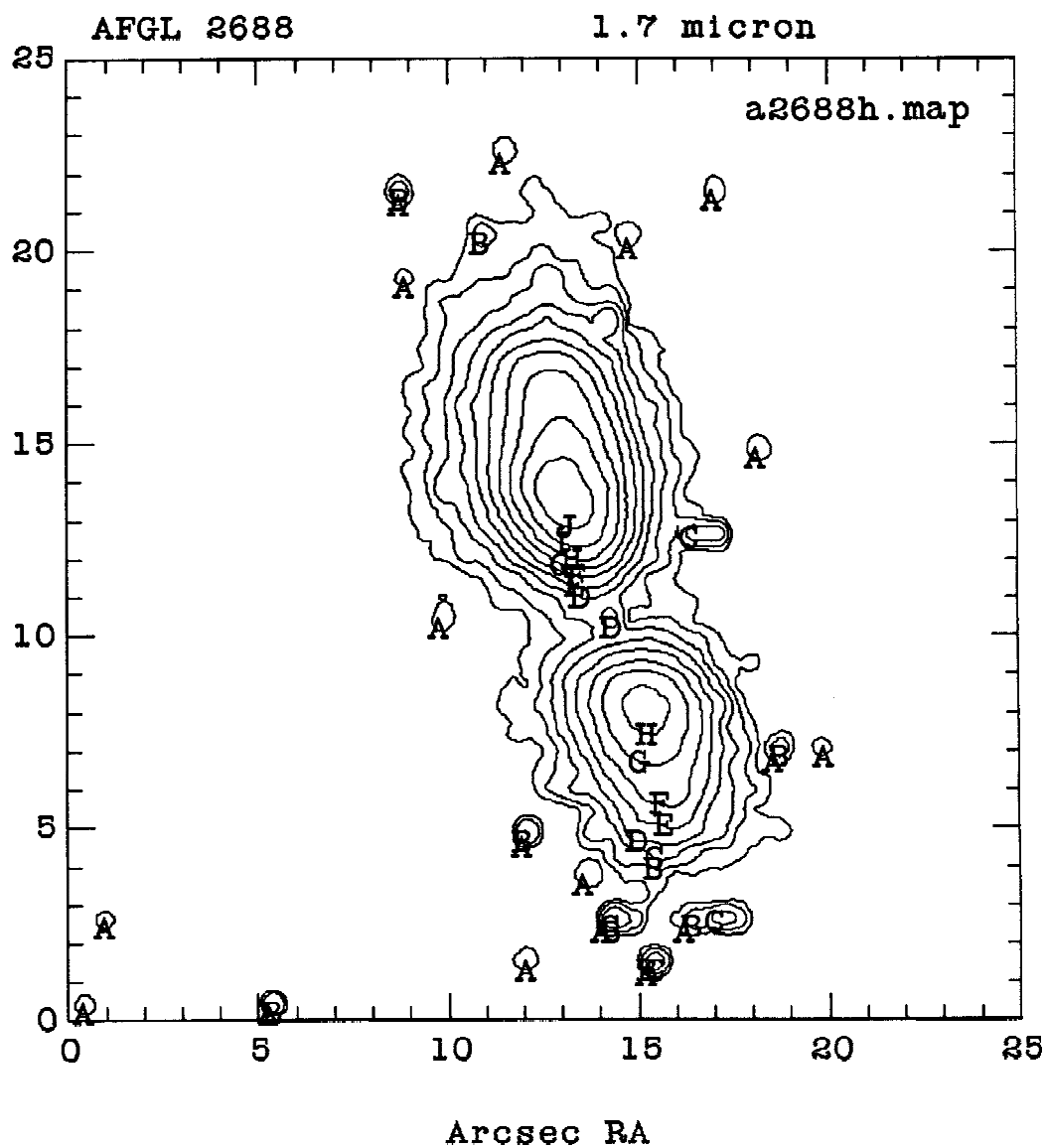
Figure 2.38b. AFGL 2688 H contour image. Contour levels are set to the following values, in mJy/arcsec^2: A = .4, B = .594, C = .883, D = 1.31, E = 1.95, F = 2.90, G = 4.30, H = 6.39, I = 9.50, J = 14.1.
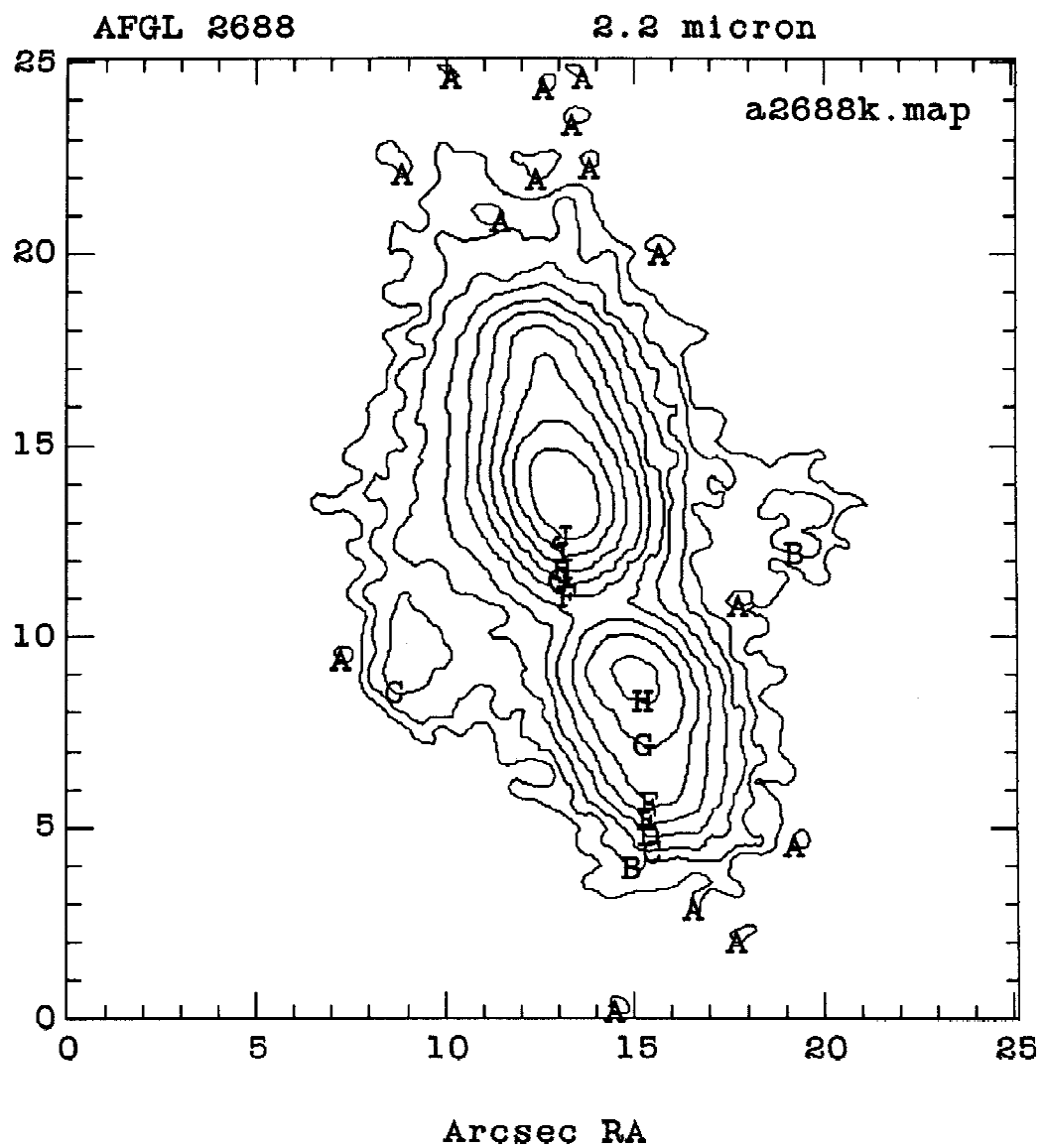
Figure 2.38c. AFGL 2688 K contour image. Contour levels are set to the following values, in mJy/arcsec^2: A = .2, B = .324, C = .523, D = .847, E = 1.37, F = 2.22, G = 3.58, H = 5.80, I = 9.39, J = 15.2.
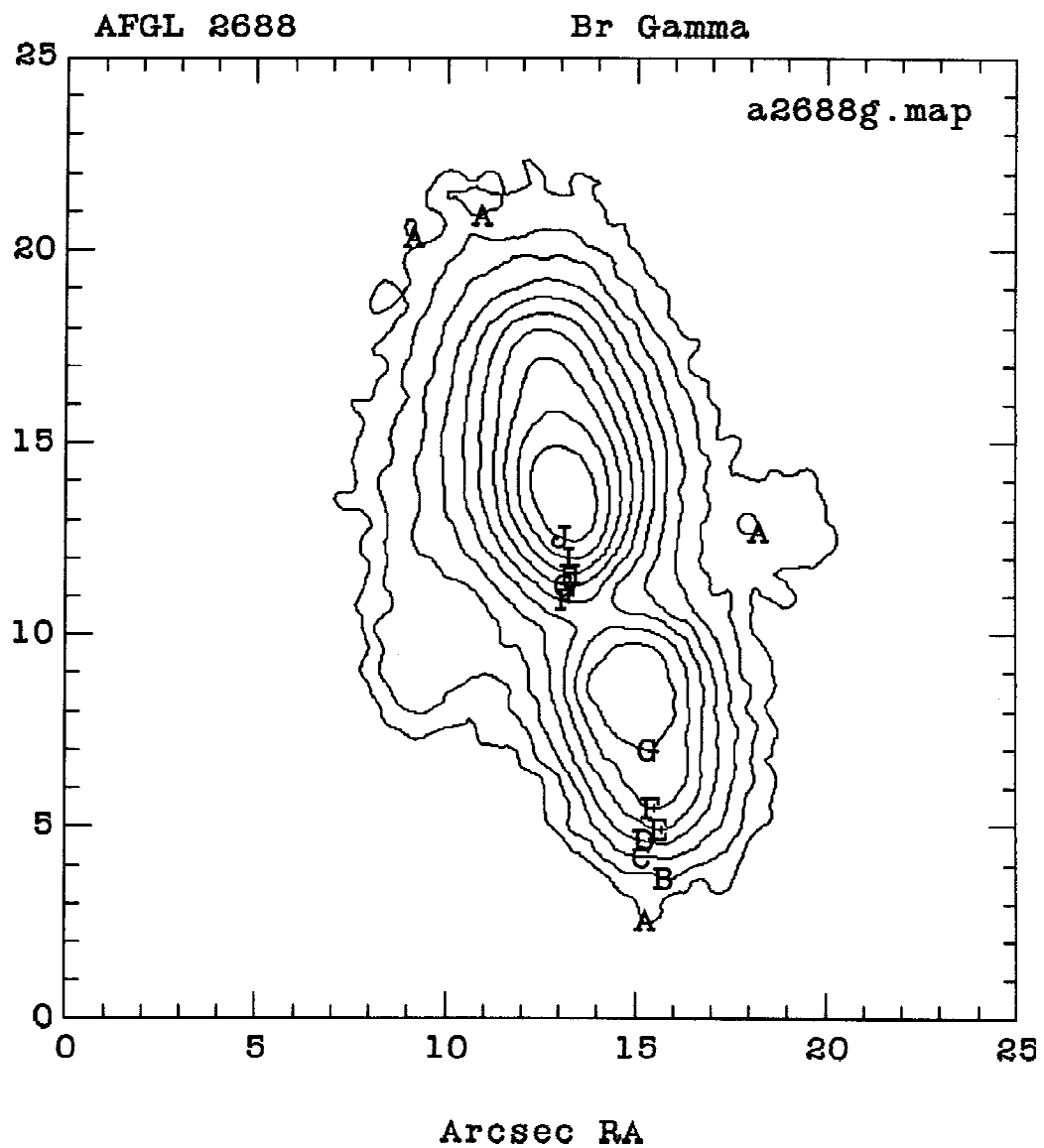
Figure 2.38d. AFGL 2688 Br γ contour image. Contour levels are set to the following values, in mJy/arcsec². A = .2, B = .324, C = .523, D = .847, E = 1.37, F = 2.22, G = 3.58, H = 5.80, I = 9.39, J = 15.2.
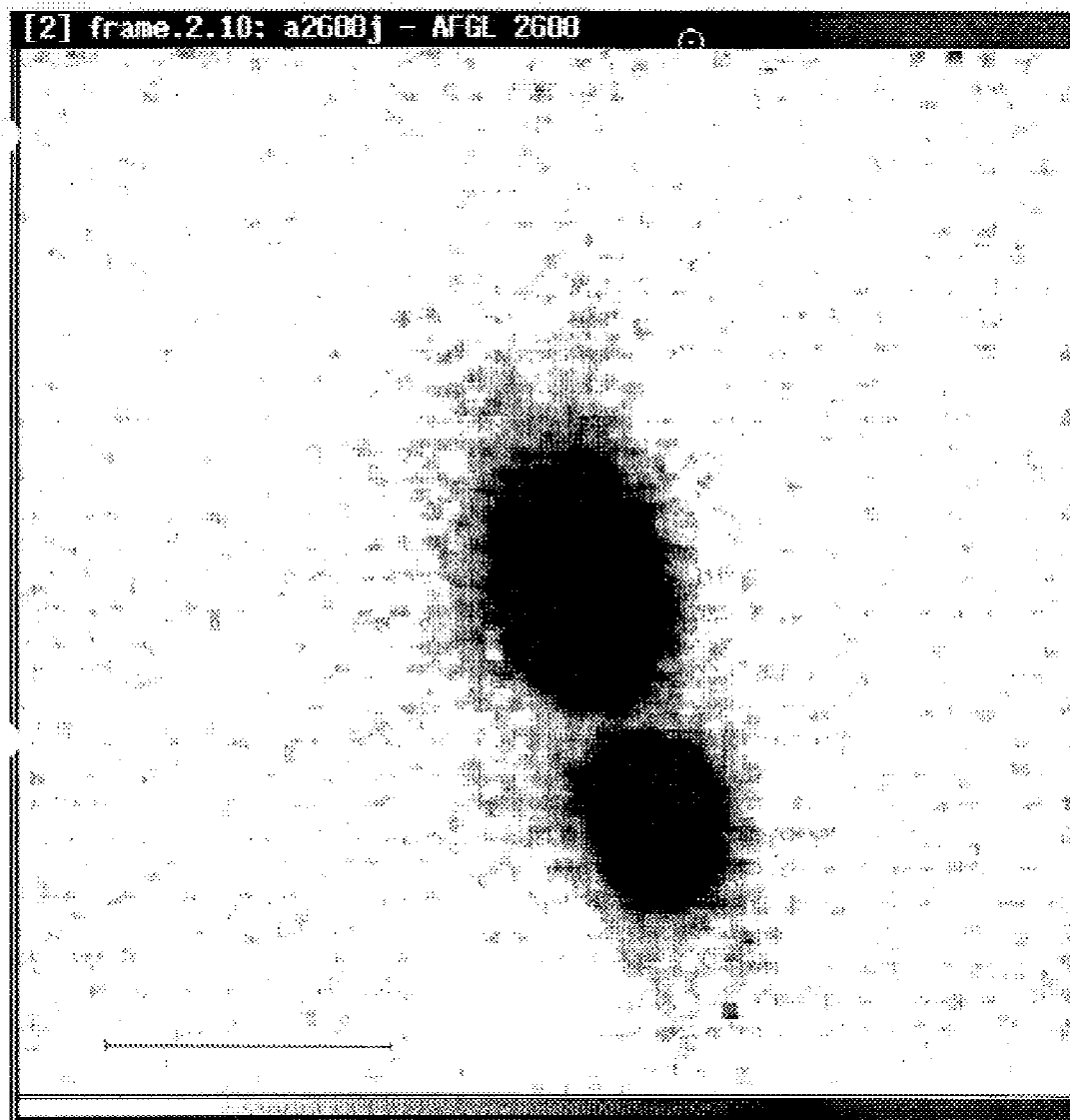
Figure 2.39. Grayscale images of AFGL 2688. The bar at the bottom of the figure has a length of 10".
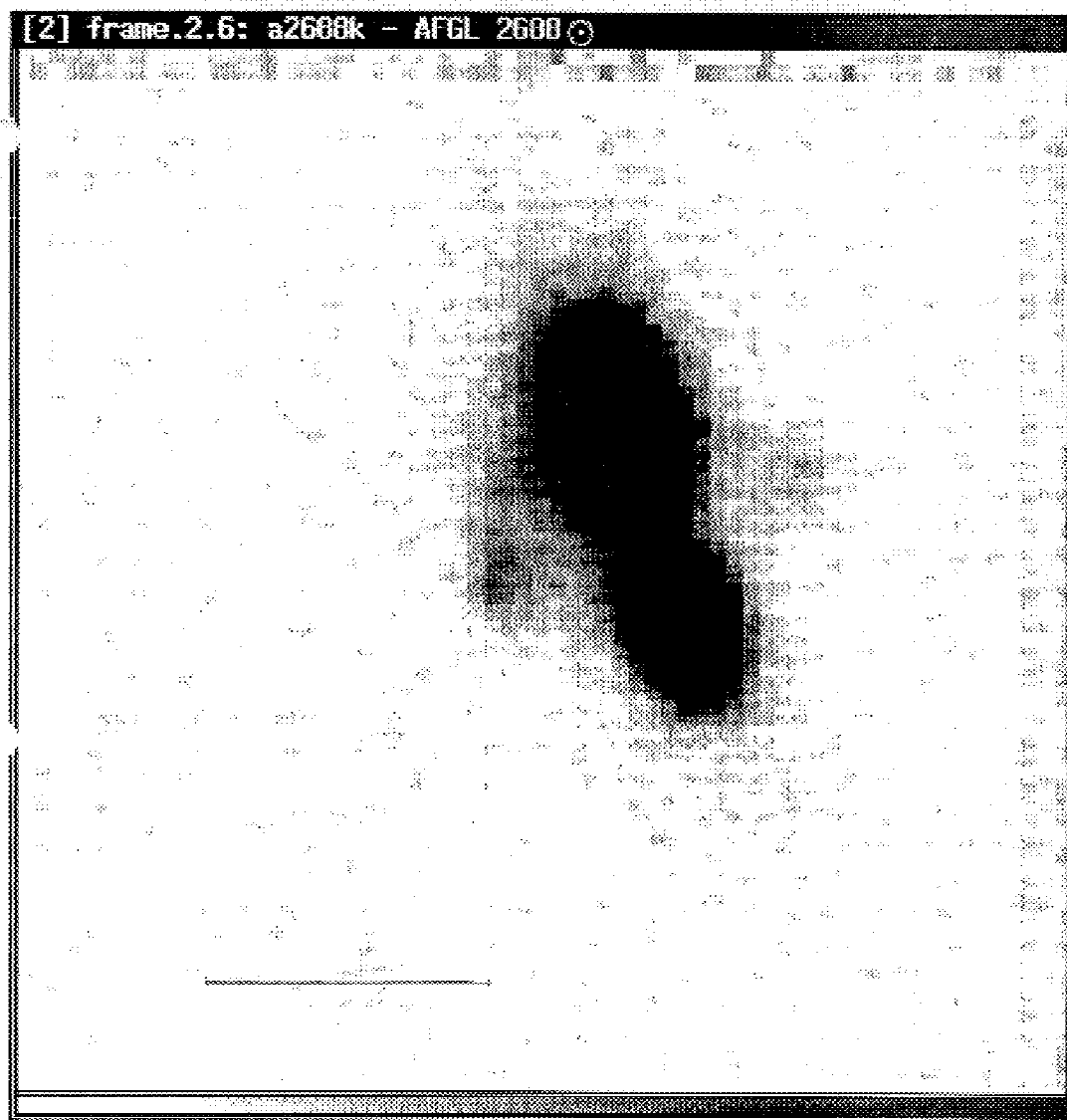2.39a. AFGL 2688 J grayscale image.
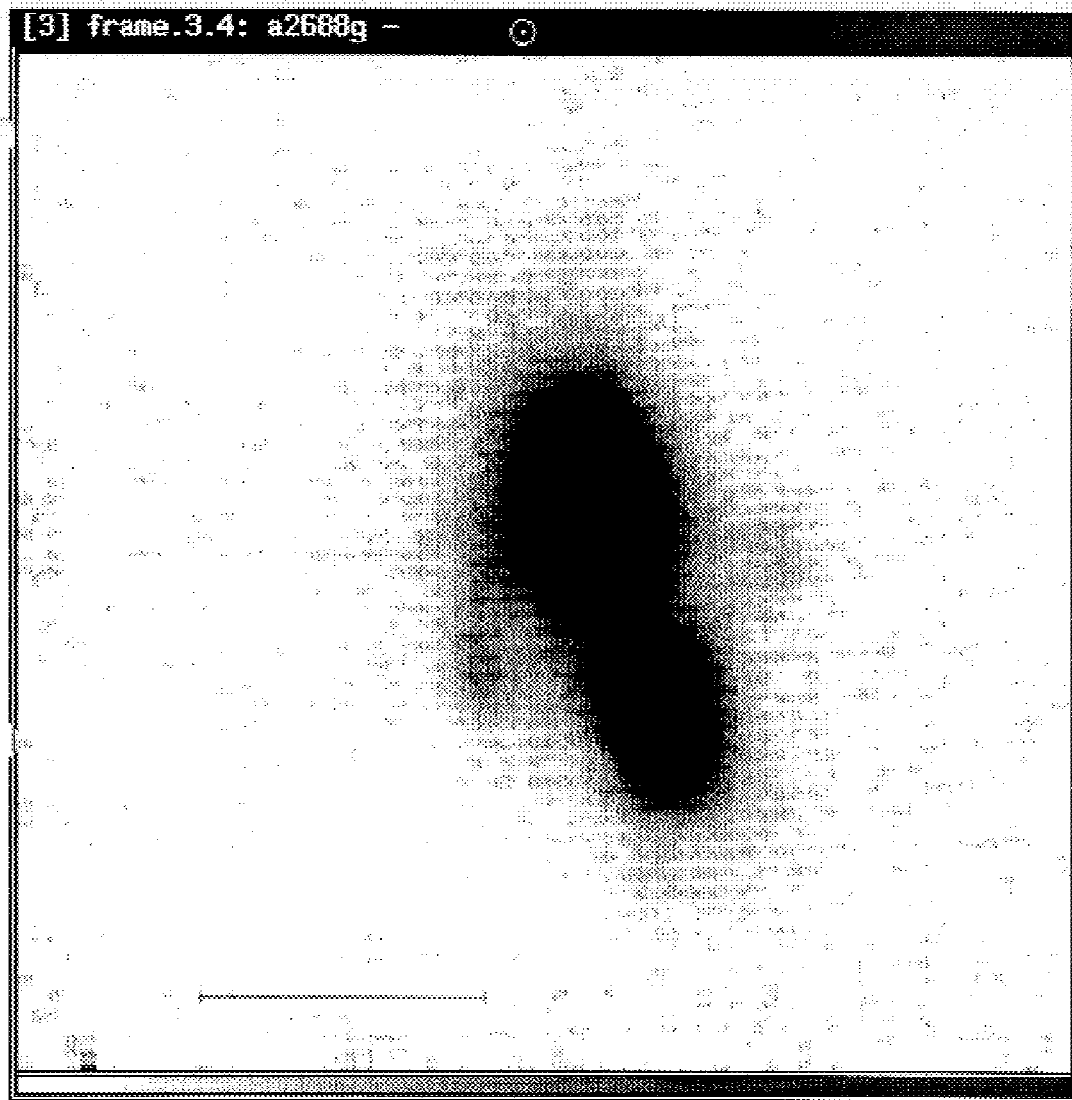
Figure 2.39b. AFGL 2688 K grayscale image.

Figure 2.39c. AFGL 2688 Br γ grayscale image.
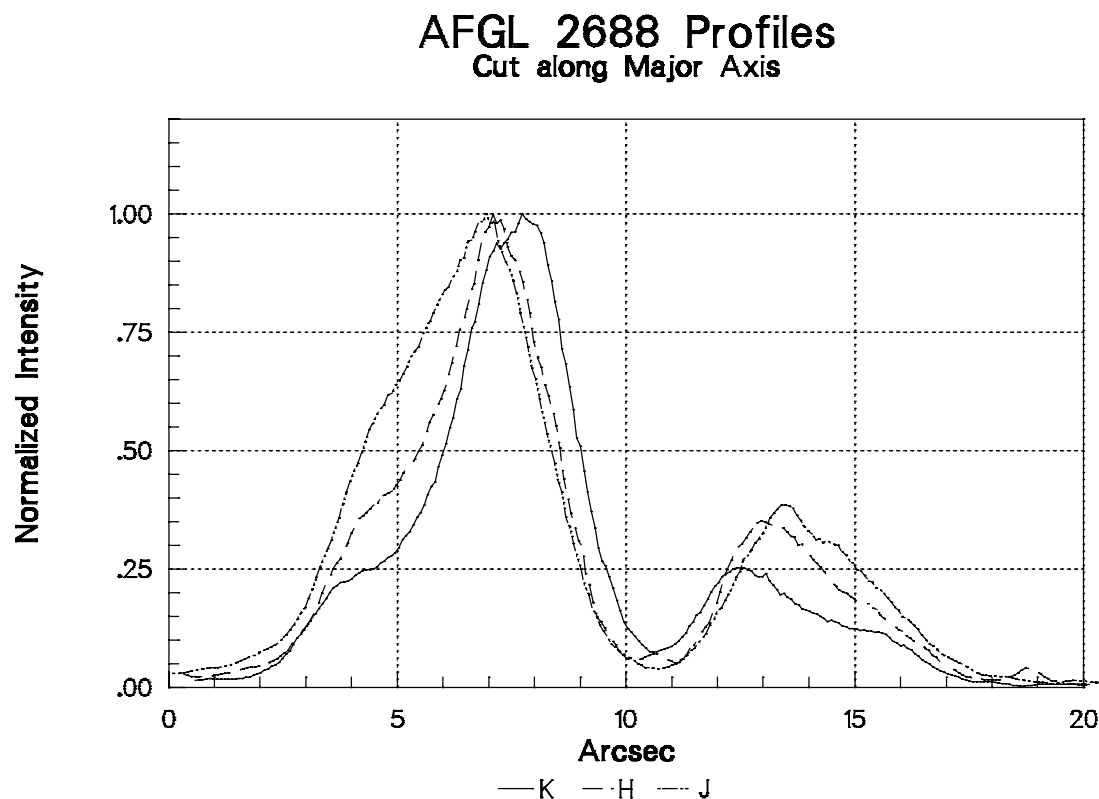
AFGL 2688 Profiles
Cut along Major Axis

Figure 2.40. Profiles through the major axis of AFGL 2688. The left side of the profile is at the NE corner of the nebula, and the right side is the the SW end of the major axis. The profiles were aligned to match the minimum between the two lobes. In the H profile, there is a small local maximum at this position. The profiles were normalized to the intensity of the brightest (NE) lobe.
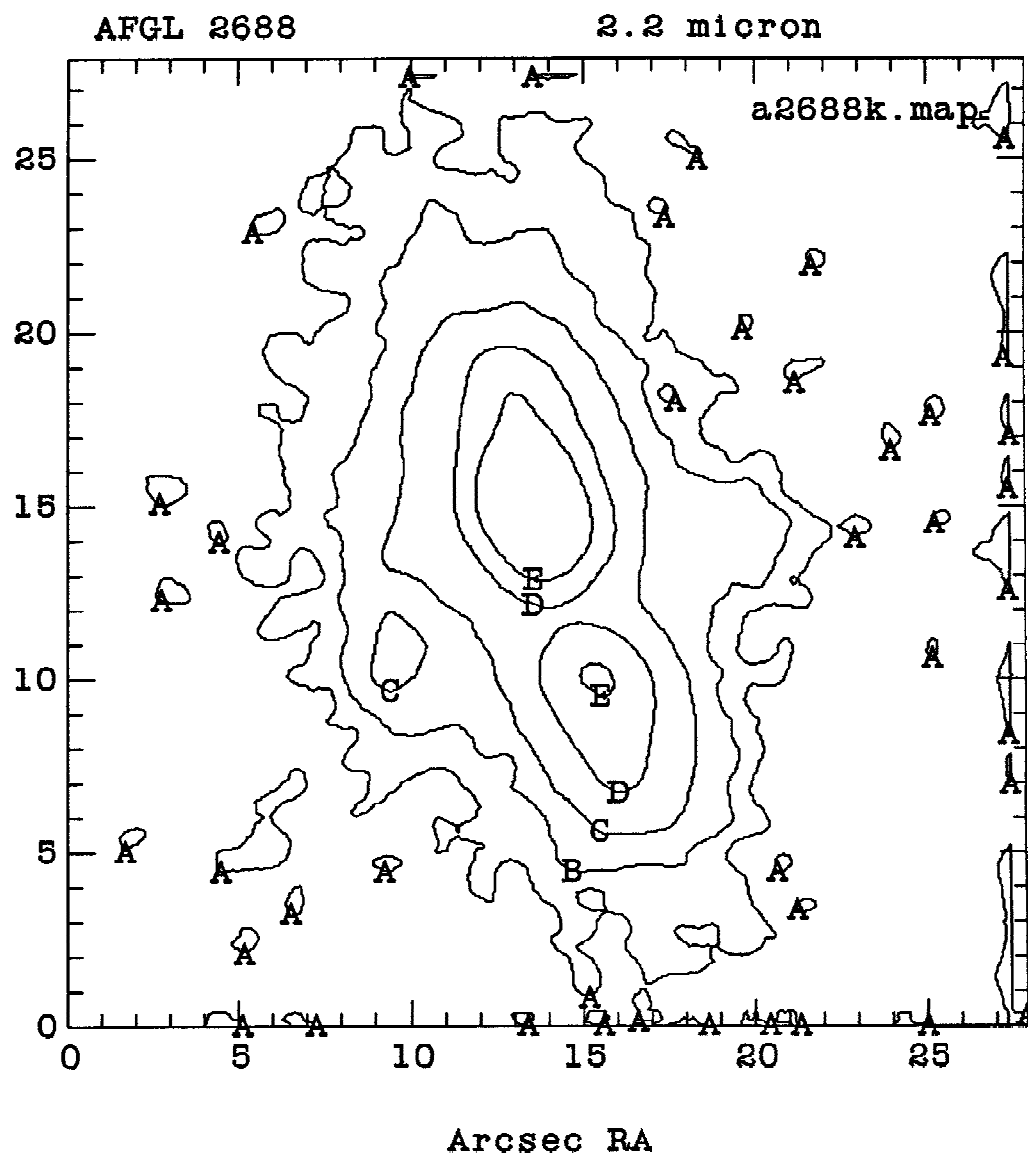
Figure 2.41. Contour image of AFGL 2688 at K showing the halo emission. This is the same data as in Figure 2.38c, which has been smoothed using a bilinear interpolation and plotted with lower contour levels. The contour levels are as follows, in mJy/arcsec^2: A = .1, B = .2, C = .523, D = 2.2, E = 5.8.
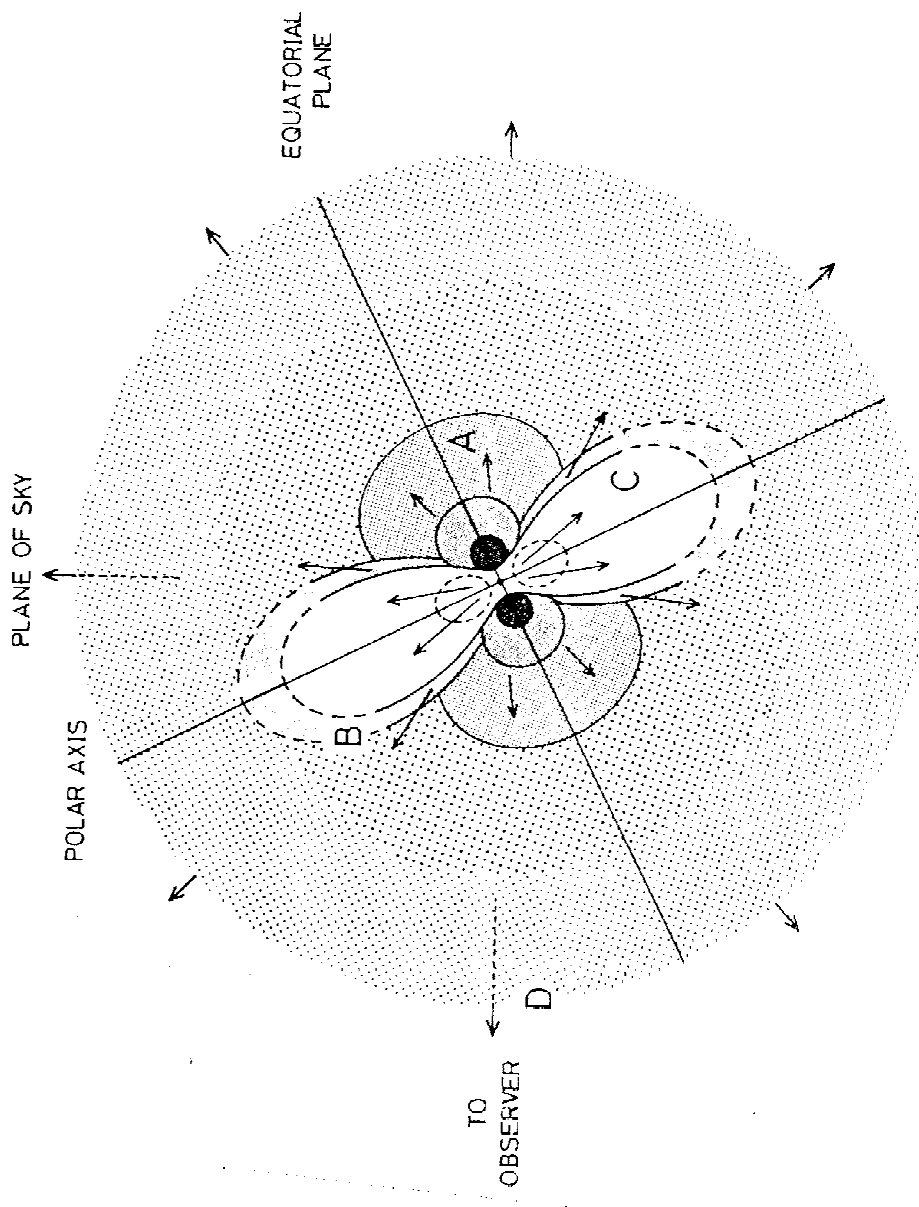
Figure 2.42. Model of AFGL 2688 from Kawabe *et al.* (1987). Region A is the expanding disk in the equatorial plane of the system. Region B shows the shells expanding in the polar direction. Region C shows the wind cavity interior to region B. Region D is the cold expanding envelope which causes the self-absorption in the source.
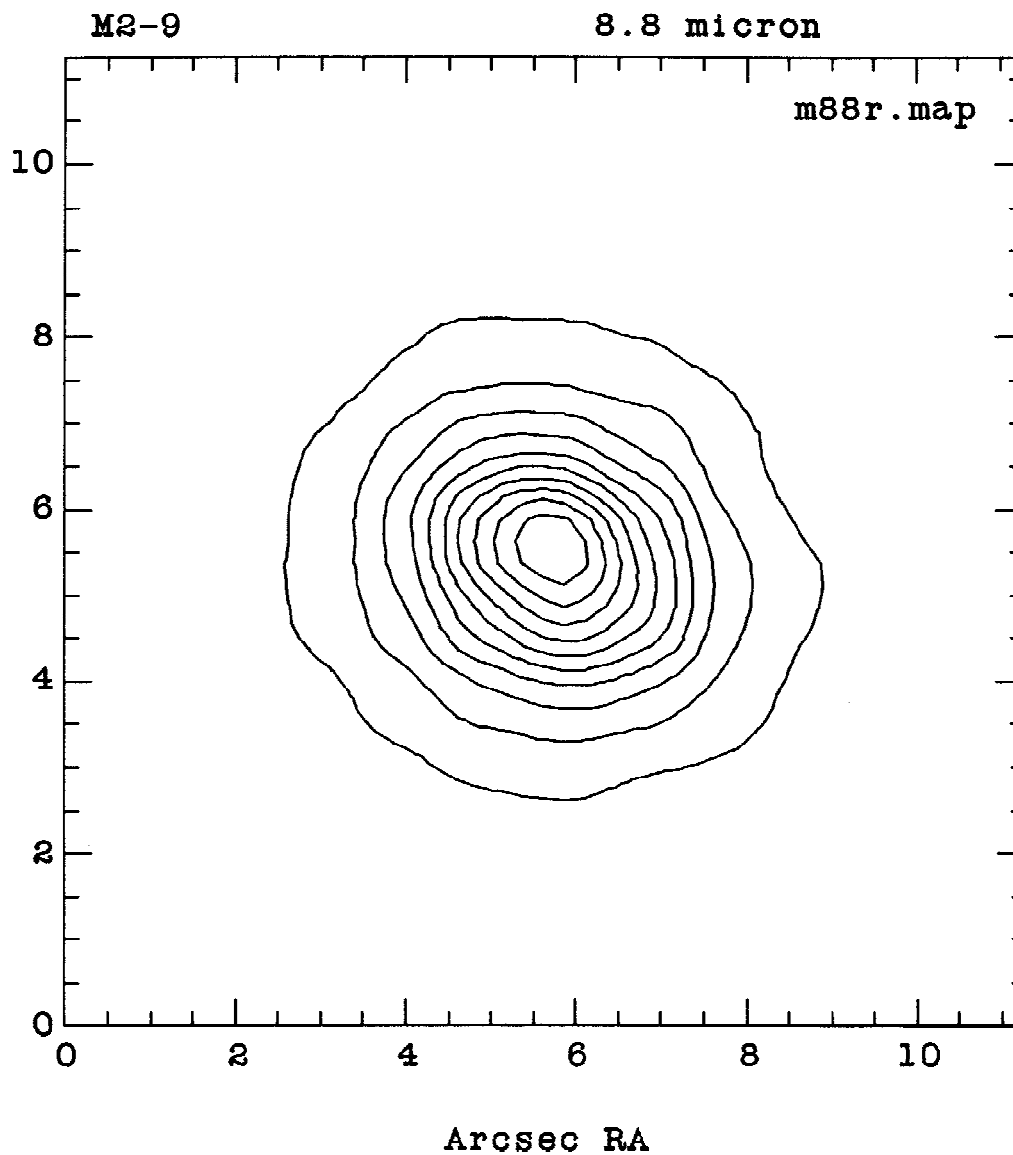
348

Figure 2.43. Mid-IR contour images of M 2-9. The contour levels are evenly spaced, as indicated below.

2.43a. Contour image of M 2-9, λ = 8.8 μm. Minimum contour level = .3 Jy/arcsec^2, contour level spacing .3 Jy/arcsec^2.
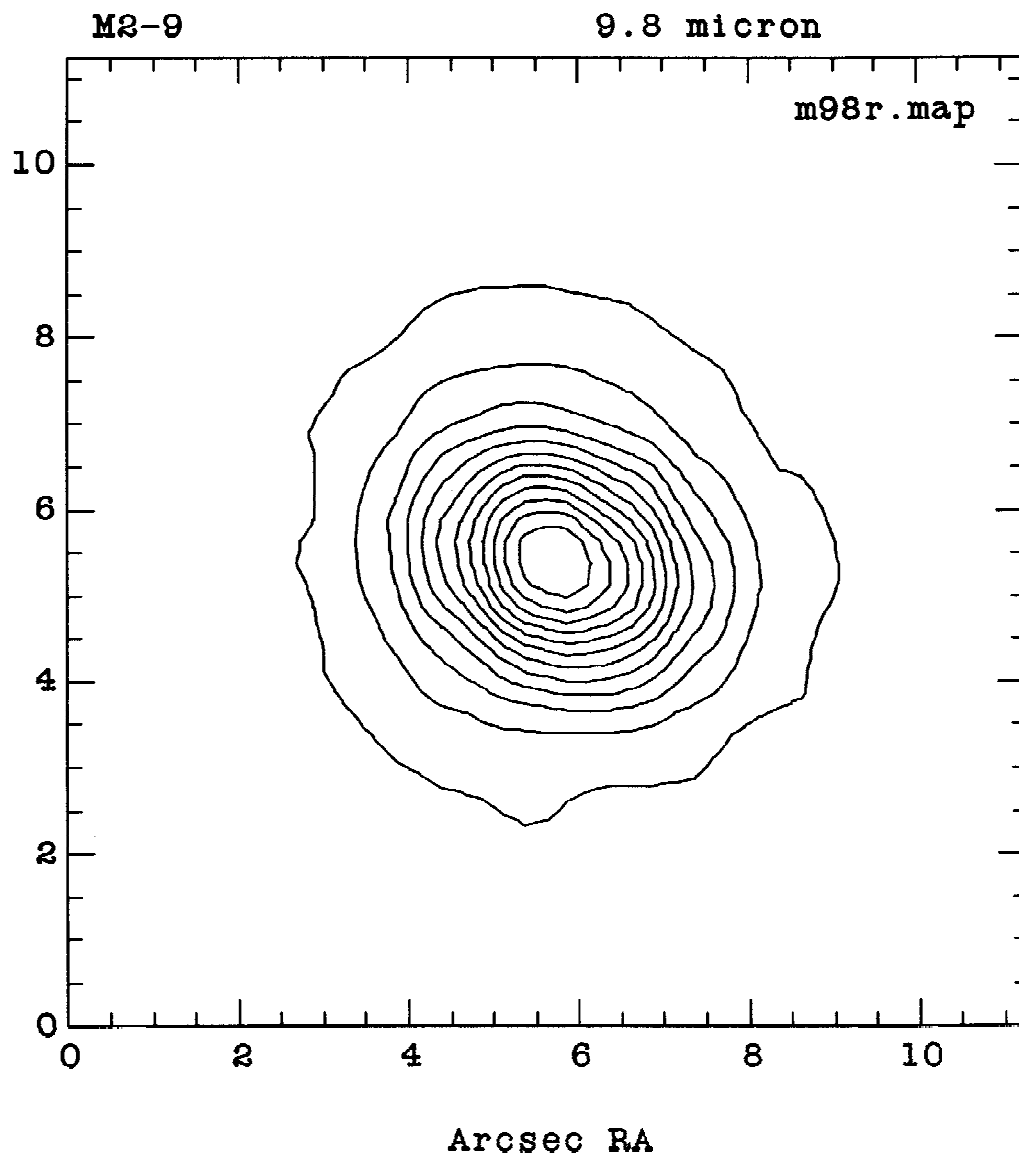
M2-9   9.8 micron

m98r.map

Arcsec RA

Figure 2.43b. M 2-9 contour image, λ = 9.8 μm. Minimum contour level = .3 Jy/arcsec², contour level spacing .3 Jy/arcsec².
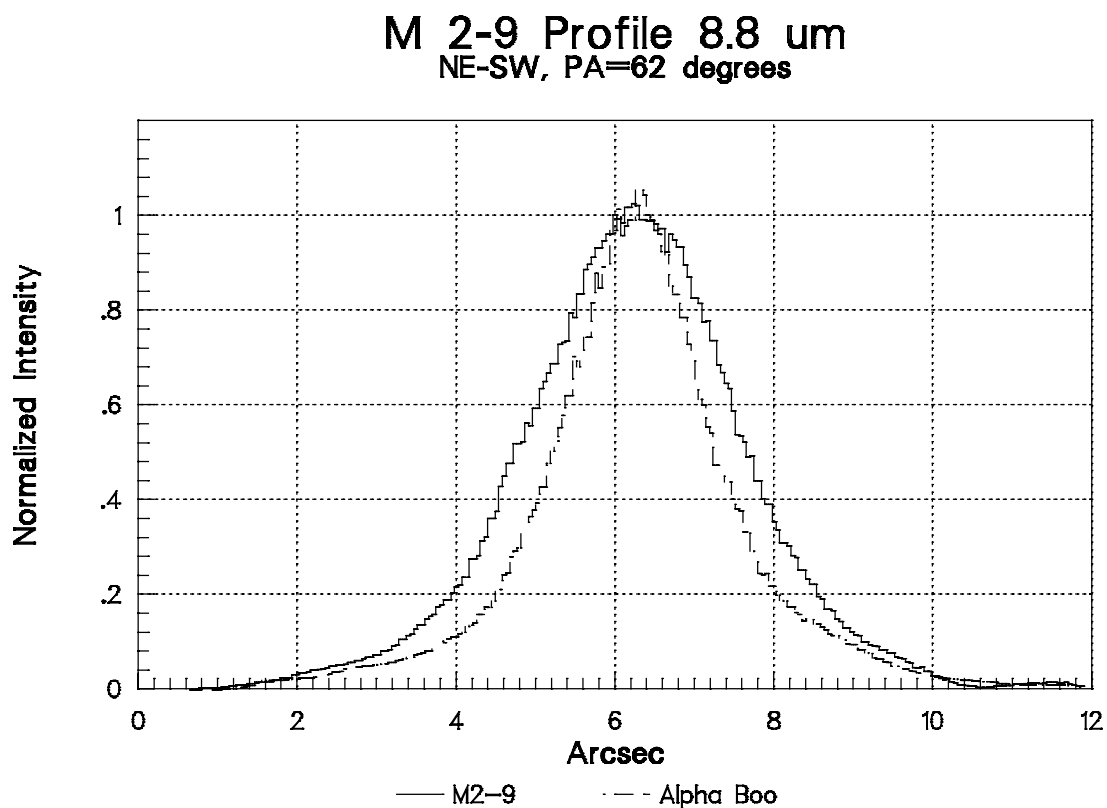
Figure 2.44. Source profiles of M 2-9 at 8.8 and 9.8 μm, with profiles of α Boo at the the same position angle for comparison. The profiles are normalized and aligned to the peak intensity value. The direction of the profiles is from NE to SW, at a PA of 62 degrees.
2.44a. Profiles of M 2-9 and α Boo at 8.8 μm.
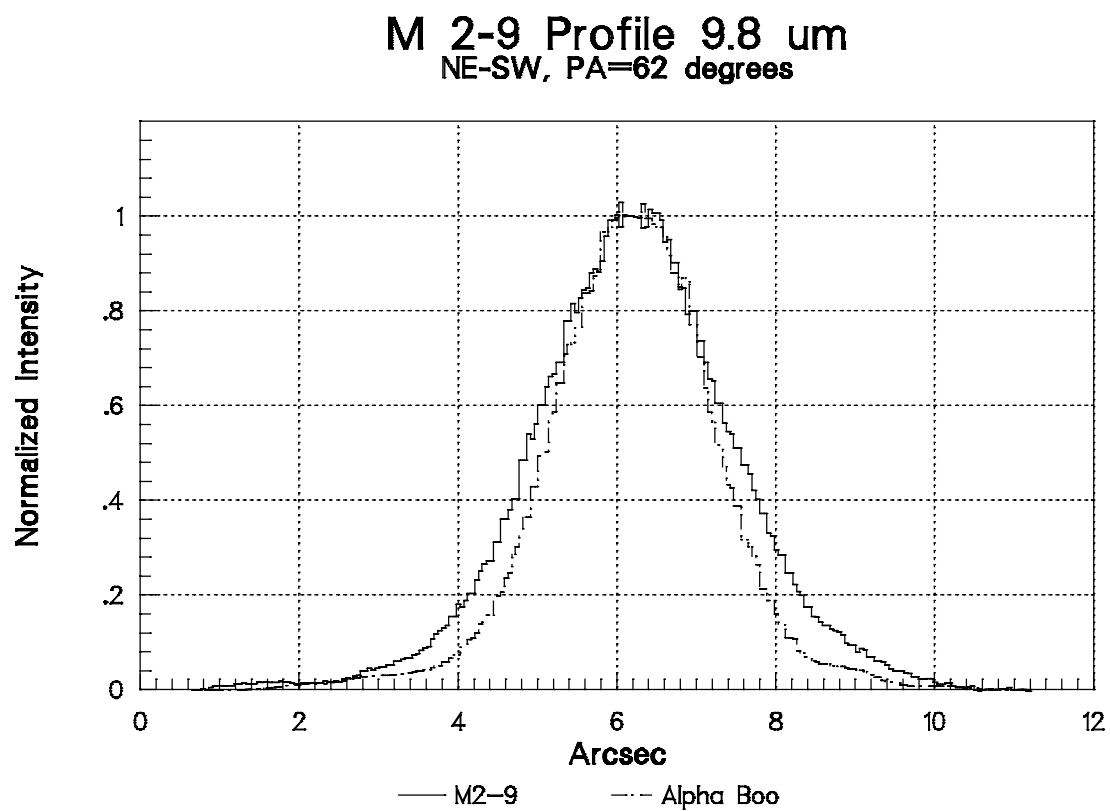
M 2-9 Profile 9.8 um
NE-SW, PA=62 degrees

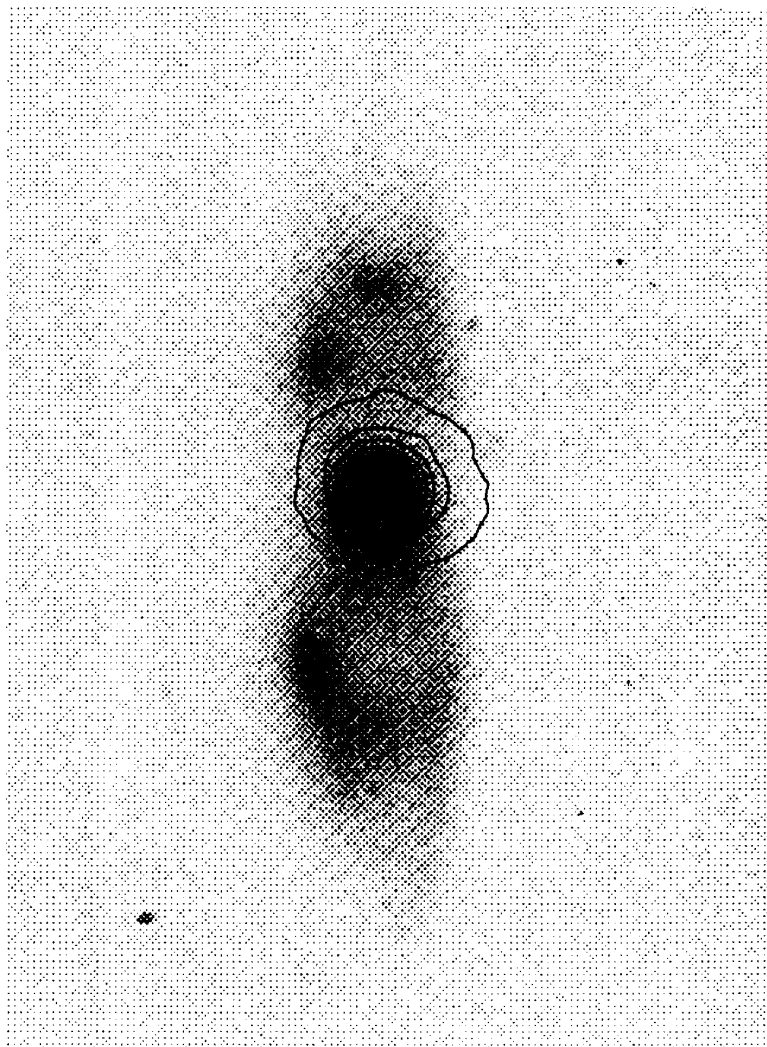Figure 2.44b. Profiles of M 2-9 and α Boo at 9.8 μm (see main caption to Figure 2.44).

Figure 2.45. Overlay of 8.8 μm image of M2-9 on negative optical image from Balick (1987). The direction of extended emission is roughly aligned with the equatorial plane of the system.
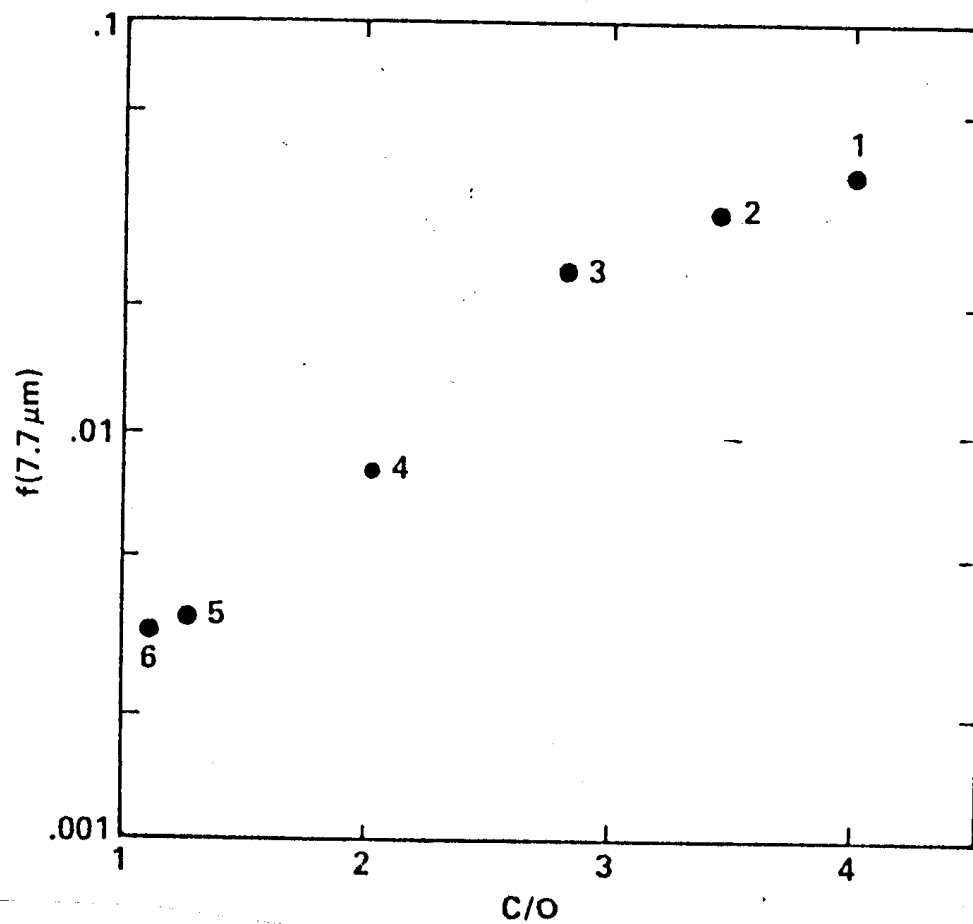
Figure 2.46. UIR correlation plot, from Cohen *et al.* (1986). This plot shows the correlation between $f(7.7\mu m)$ (the fraction of nebular far-IR luminosity radiated by the 7.7 μm UIR band), and the nebular C/O ratio.